AD-A129 715 FUSION WELDING RESEARCH(U) MASSACHUSETTS INST OF TECH 1/1
CAMBRIDGE DEPT OF MATERIALS SCIENCE AND ENGINEERING
T W EAGAR ET AL. 30 APR 83 N00014-80-C-0384

UNCLASSIFIED F/G 13/8 NL

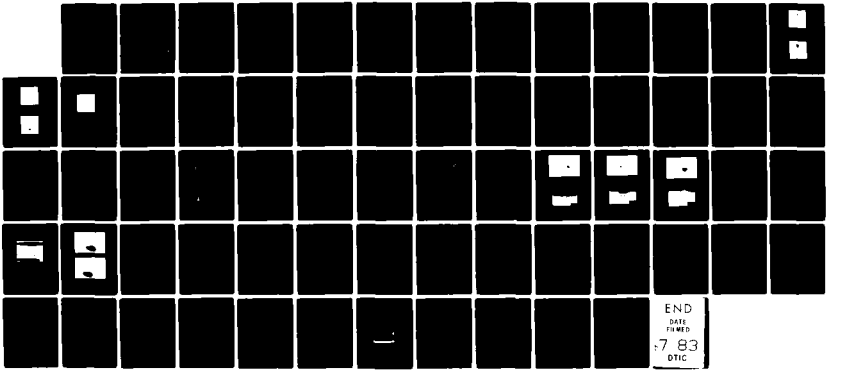

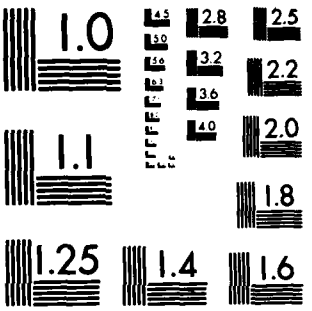

SECURITY CLASSIFICATION OF THIS PAGE (When Data Entered)

(12)

REPORT DOCUMENTATION PAGE

READ INSTRUCTIONS BEFORE COMPLETING FORM

1 REPORT NUMBER	2 GOVT ACCESSION NO: AD-A129715
3 RECIPIENT'S CATALOG NUMBER	
4 TITLE (and Subtitle): FUSION WELDING RESEARCH	5 TYPE OF REPORT & PERIOD COVERED: 3rd annual technical report April 30, 1983
6 PERFORMING ORG. REPORT NUMBER	
7 AUTHOR(s): T. W. Eagar, G. B. Hunter, G. J. Dunn, C. D. Sorensen, A. Block-Bolten, M.-L. Lin, S. K. Fan, G. D. Ries, C. Allemand, B. Wilson, A. Oladipupo and R. Schoder	8 CONTRACT OR GRANT NUMBER(s): N00014-80-C-0384
9 PERFORMING ORGANIZATION NAME AND ADDRESS: Department of Materials Science & Engineering, Massachusetts Institute of Technology, Cambridge, MA 02139	10 PROGRAM ELEMENT, PROJECT, TASK AREA & WORK UNIT NUMBERS
CONTROLLING OFFICE NAME AND ADDRESS: Dr. Bruce A. MacDonald, Office of Naval Research, Arlington, VA 22217	12 REPORT DATE: April 30, 1983
	13 NUMBER OF PAGES: 62
14 MONITORING AGENCY NAME & ADDRESS (if different from Controlling Office)	15 SECURITY CLASS. (of this report): Unclassified
	15a DECLASSIFICATION/DOWNGRADING SCHEDULE

16 DISTRIBUTION STATEMENT (of this Report)

Reproduction in whole or in part is permitted for any purposes of the United States Government. Distribution of this document is unlimited.

17. DISTRIBUTION STATEMENT (of the abstract entered in Block 20, if different from Report)

18. SUPPLEMENTARY NOTES

19 KEY WORDS (Continue on reverse side if necessary and identify by block number)

20 ABSTRACT (Continue on reverse side if necessary and identify by block number)

This report summaries progress during the third year of research on the physics of arc welding processes. Studies include vapor emission from weld pools, development of a high speed infrared temperature monitor, digital signal analysis of weld noise voltages, convection and surface depression of the weld pool, electroslag welding of titanium, pulsed current gas metal arc welding and fracture toughness of HY-80 weldments.

DD FORM 1 JAN 73 1473 EDITION OF 1 NOV 65 IS OBSOLETE
S/N 0102-014-6601

SECURITY CLASSIFICATION OF THIS PAGE (When Data Entered)

FUSION WELDING RESEARCH

by

T. W. Eagar G. B. Hunter, G. J. Dunn
C. D. Sorenson, A. Block-Bolten, M.-L. Lin,
S. K. Fan, G. D. Ries, C. Allemand, B. Wilson,
A. Oladipupo and R. Schoder

Third Annual Technical Report
Contract N00014-80-C-0384

to

Office of Naval Research
Department of the Navy
Arlington, VA 22217

ATTN: Dr. Bruce MacDonald

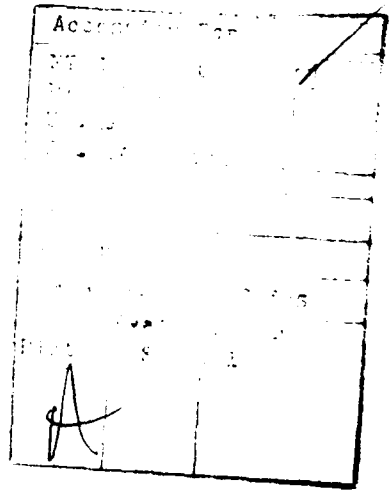

April 30, 1983

TABLE OF CONTENTS

FUSION WELDING RESEARCH

ABSTRACT

This report summaries progress during the third year of research on the physics of arc welding processes. Studies include vapor emission from weld pools, development of a high speed infrared temperature monitor, digital signal analysis of weld noise voltages, convection and surface depression of the weld pool, electroslag welding of titanium, pulsed current gas metal arc welding and fracture toughness of HY-80 weldments.

I. INTRODUCTION

This report describes work performed in the MIT Welding Laboratory under Office of Naval Research sponsorship. The work is generally fundamental in nature, but attempts have been made to interface the studies with several specific U.S. Navy programs. The best example of these directed programs include evaluation of the fracture toughness of HY-80 weld metal. Direct contact with DTNSRDC-Annapolis, General Dynamics/Electric Boat Division and Alcoa Technical Center has been helpful for several of the studies. Each of these three laboratories has contributed in some manner to the progress reported here through either consultation, materials and/or services.

The research conducted from 15 February 1982 to 14 February 1983 can broadly be divided into four main topics, viz.

1. Spectrographic studies of the arc and weld pool,
2. Joining of heavy section titanium,
3. Fracture toughness of HY-80 weld metal,
4. Sensors for automation of arc welding.

II. SPECTROSCOPY OF ARC WELDING

Spectroscopic studies of the arc welding process performed during the past contract year include vapor emission from weld pools and development of a multichannel Infrared-Red Temperature Micro-Analyzer. As noted in our previous report (1), these two analyses are coupled through a thermodynamic upper-bound analysis which has been published recently (2). Another paper expanding on this previous work has been drafted during the current contract year and should be submitted for publication shortly. A brief description of the results of the two studies noted above are given below.

A. Vapor Emission from the Weld Pool

Dr. C. Allemand and Mr. G. J. Dunn

During the previous reporting period, it was noted that calcium metal vapors were present in the welding arc. This is of considerable concern since calcium has a low ionization potential and even small quantities of this element might significantly alter the electrical properties of the plasma

In order to learn more about the effects of calcium, three different heats of 304 stainless steel with controlled additions of Ca and S were obtained from Republic Steel Corporation Research. The compositions of these steels were similar except for a high concentration of calcium in one (W167A) and a high concentration of sulphur in another (W156). Spectra over a wide range of wavelengths were recorded from arcs on these steels. Figures 1 through 3 show spectra for the three steels between 385 and 425 nm. It can be seen that the steel with a high sulphur content (Figure 2) exhibits increased vaporization of manganese, iron and chromium. Also,

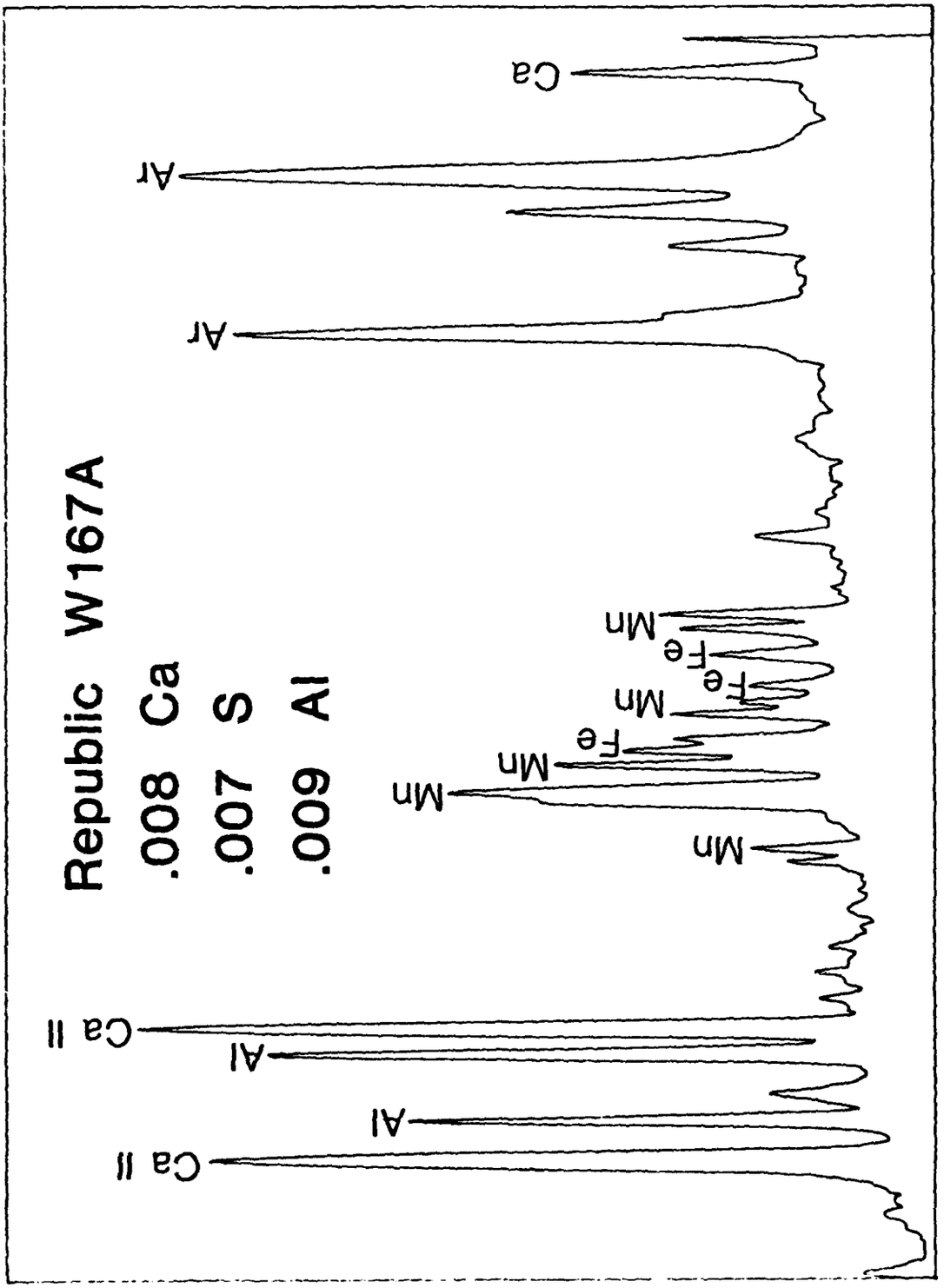
Republic W167A
.008 Ca
.007 S
.009 Al
Ca II
Al
Al
Ca II
Mn
Mn
Fe
Mn
Fe
Fe
Mn
Ar
Ar
Ca

Figure 1

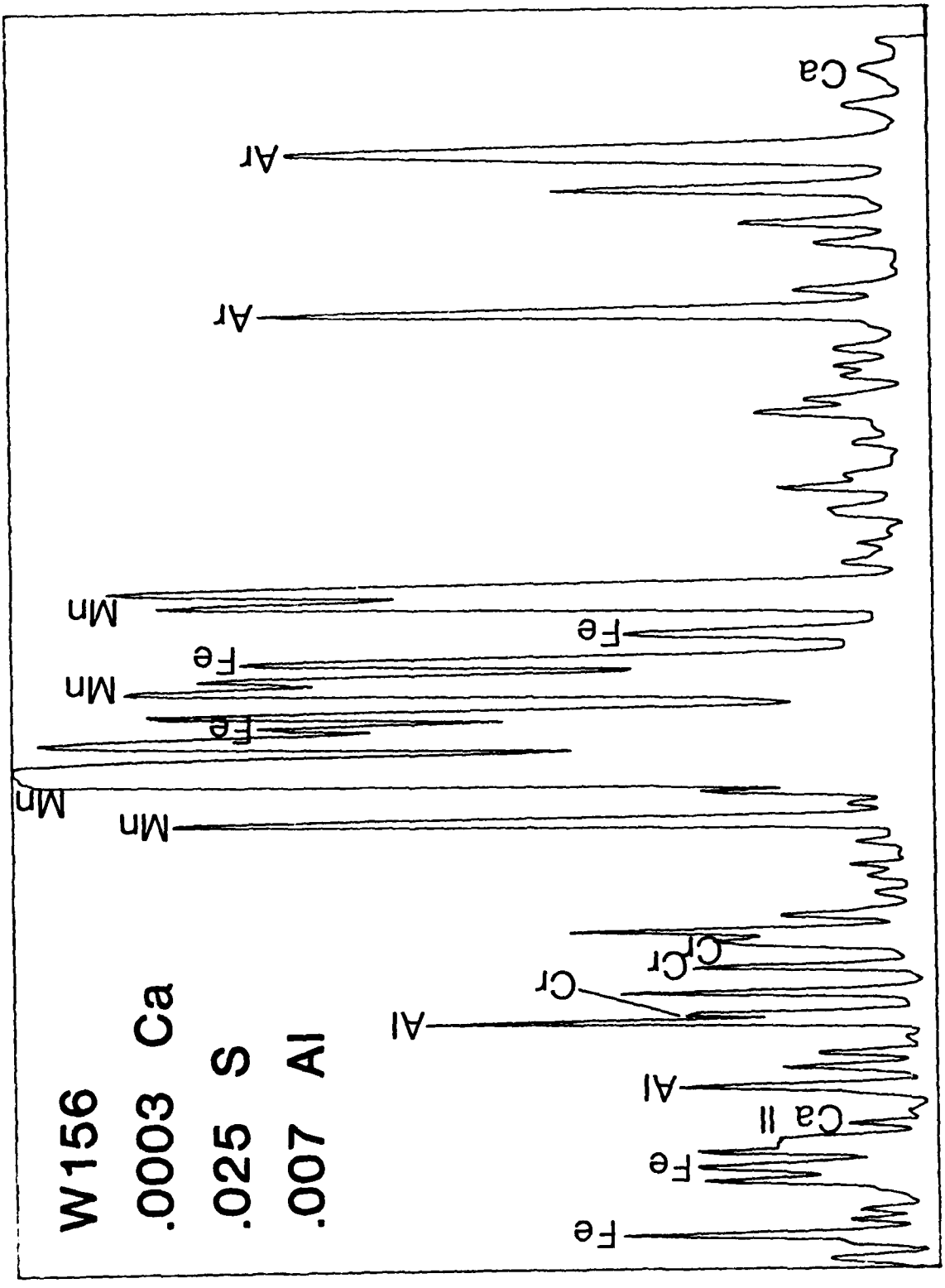
W156
.0003 Ca
.025 S
.007 Al
Fe
Ca II
Al
Al
Cr
Cr
Cr
Mn
Mn
Fe
Mn
Fe
Mn
Fe
Ar
Ar
Ca

Figure 2

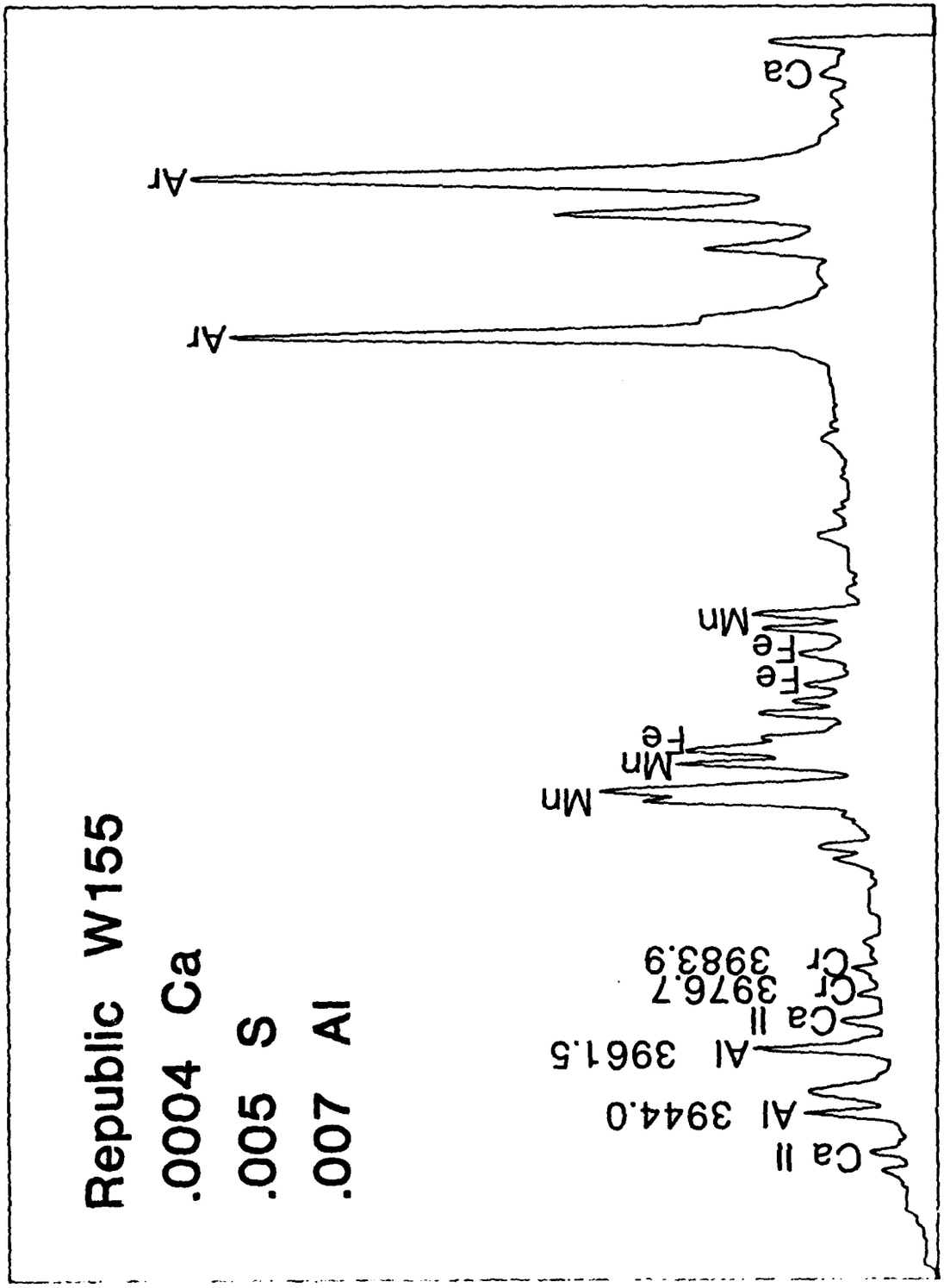
Republic W155
.0004 Ca
.005 S
.007 Al
Ca II
Al 3944.0
Al 3961.5
Ca II
Cr 3976.7
Cr 3983.9
Mn
Mn
Fe
Fe
Fe
Mn
Ar
Ar
Ca

Figure 3

the steel with a high calcium content (Figure 1) produces a significantly greater amount of calcium vapor in the arc, and also a greater amount of aluminum vapor, although the aluminum content of this steel is close to that of the others.

It was also discovered that calcium and aluminum may enter the arc from the tungsten electrode. Figure 4 shows a spectrum recorded from an arc struck between two electrodes. The strength of the calcium and aluminum lines indicate that a significant portion of the calcium vapor in the arc may be emitted from the electrode.

In order to determine the distribution of metal vapors in the arc, a double monochromator was modified to examine a monochromatic, two-dimensional image of the arc. Figures 5 through 9 show monochromater photographs of 100A helium arcs on 304 stainless steel (Sample W156). These photographs are produced solely by light of a characteristic wavelength for the element indicated. Thus, each photograph is a "mapping" of vapor distribution in the arc. It is seen in Figure 5 that Mn vapor appears to be swept away from the pool and attracted back to the electrode while the other vapors are generally concentrated at the weld pool. (The bright electrode in Figure 6 is due to a longer exposure time necessary to resolve Al vapor).

At the present time we are developing a mathematical model of the welding arc. This model will determine the effects of metal vapors on the thermal and electrical properties of the plasma; and subsequently on the current distribution in the arc. By this model we hope to explain the mechanism by which minor element vapors affect weld quality.

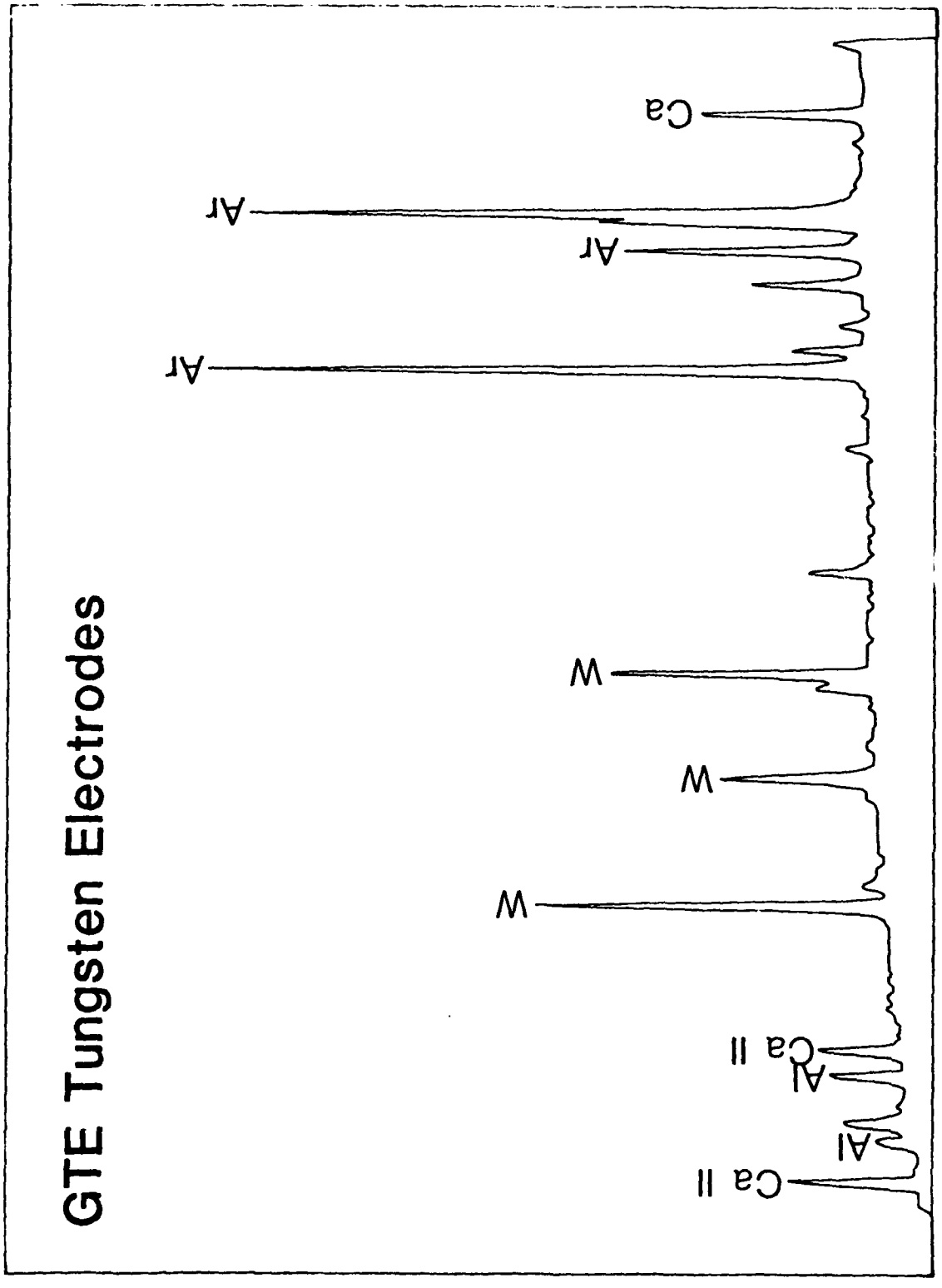

Figure 4

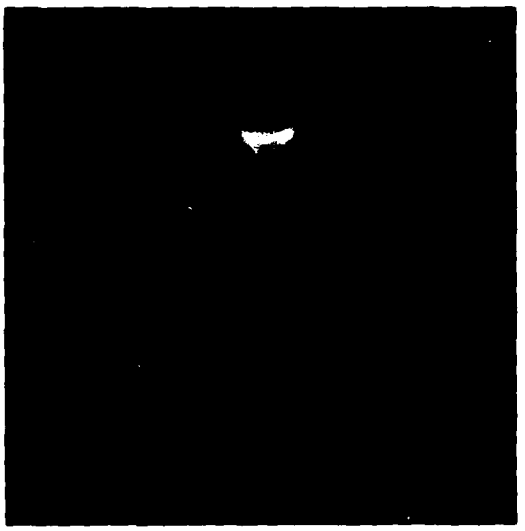

Figure 5: Manganese vapor at 4033 Å wavelength 100 amperes
Helium shielding

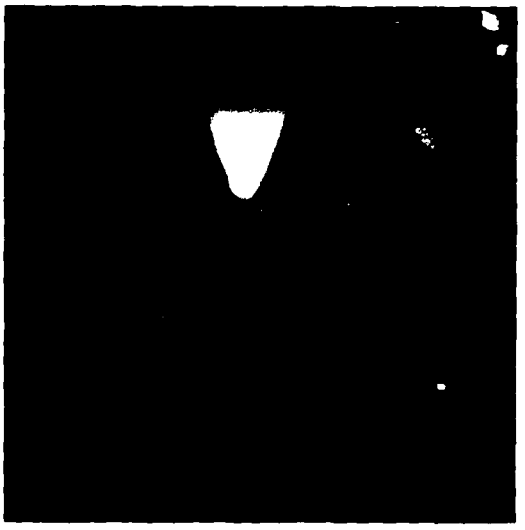

Figure 6: Aluminum ion vapor at 6201 Å wavelength 100 amperes

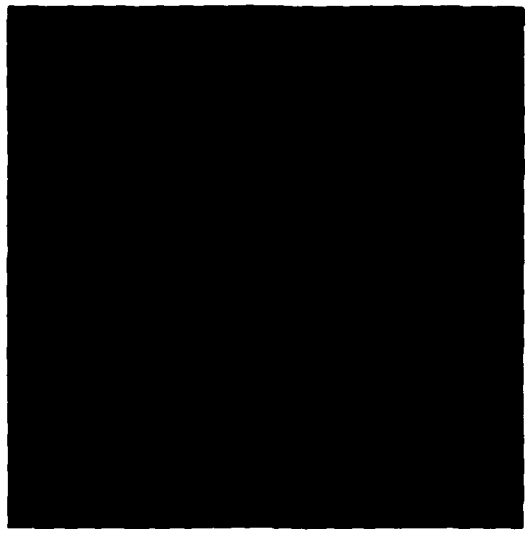

Figure 7: Iron vapor at 12,359 Å wavelength 100 amperes

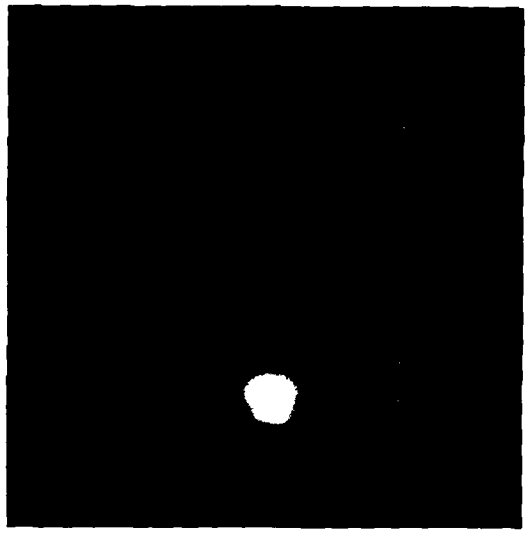

Figure 8: Calcium ion vapor at 12,599 Å wavelength 100 amperes

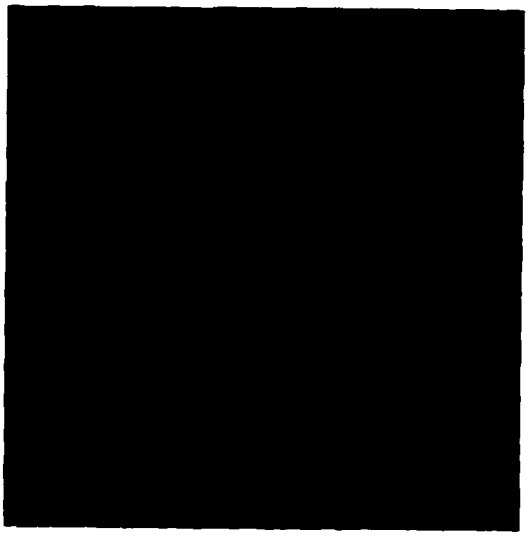

Figure 9: Chromium at 4274 Å wavelength 100 amperes

B. Infrared Measurement of the Weld Pool Surface Temperatures

Mr. G. B. Hunter and Dr. C. Allemand

A system to measure temperatures across a weld pool surface would greatly aid the study of heat transport, fluid convection, and metal vaporization in arc weld pools. The design of such a system has proceeded based on an infrared microscope, Optical Multichannel Analyzer (OMA), and a DEC MINC 11/23 minicomputer. The purchase and construction of most of the major components, and the development of the computer software for calibration and temperature calculation had been previously completed. Therefore, it was hoped that the Multichannel Infrared-Red Temperature Micro-Analyzer (MIRTMA) system could be demonstrated on a black body radiation source and then on a weld pool during this past year. However, complications involving the use of the OMA detector for precision measurements have necessitated the development of additional calibrations and the purchase of additional equipment.

The basic method involves measuring the spectral radiance at 500 different wavelengths for each 0.1 mm spot in a raster scan of the pool surface and calculation of the temperature of each spot. A Planck radiation law curve, assuming a particular emissivity function, is fitted to the spectral radiance vs. wavelength data to determine the temperature and emissivity. Wavelength is calibrated using a mercury light with spectral peaks at known wavelengths. The calibration of spectral radiance has caused the problems that have slowed the project. These problems and many of their solutions will be described subsequently.

A standard lamp of spectral radiance with calibrated values traceable to NBS standards is used to calibrate the OMA signal with spectral radiance.

The lamp contains a flat tungsten ribbon which is placed in the location that will be occupied by the source (the black body or weld pool). The calibrated values of the lamp are divided by the OMA signals measured while viewing the lamp ribbon with the infrared microscope to obtain a calibration constant for each channel. Assuming a linear detector response with light intensity, these constants can then be multiplied by the OMA signals as measured while viewing a radiation source to obtain the spectral radiance values for the source.

This procedure places certain requirements and restrictions on the MIRTMA system. First, the lamp must be powered with a constant current supply regulated within $\pm 0.1\%$ in order to obtain the calibrated spectral radiance values. Second, a cut-off filter is ncessary to eliminate second or higher order radiation from the measurements since such radiation would make calibration extremely difficult. A cut-off filter of 600 nm for the system wavelength range of 600-1200 nm was chosen for this purpose. This range is suitable for weld pools and for the standard lamp (see Figure 10). Third, the detector must be gated or the source radiation chopped so that measurements can be made within the time constant of a source spot. For the weld pool, this time constant could be less than 100 microseconds, thus eliminating most choppers from consideration since they are too slow. Because of the short viewing time and gating requirements, a gatable intensified detector becomes very attractive.

Currently a Silicon Intensified Target (SIT) vidicon detector is being used with the OMA. This detector can be gated at less than 1 microsecond and has an intensified sensitivity for a wavelength range of 350-850 nm with a S20 photocathode response (see Figure 11). Since a longer wavelength

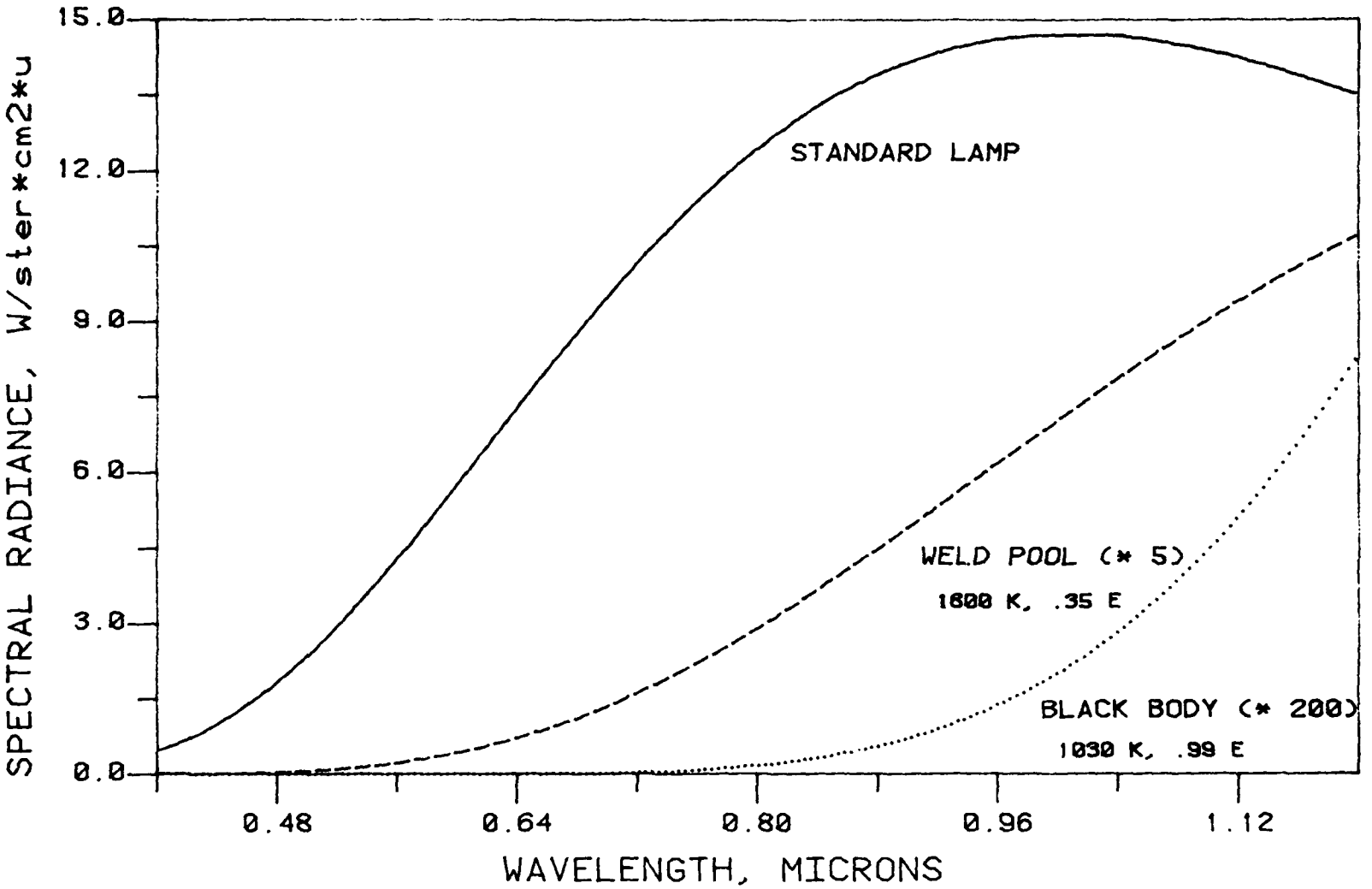

COMPARISON OF RADIATION SOURCES

Figure 10

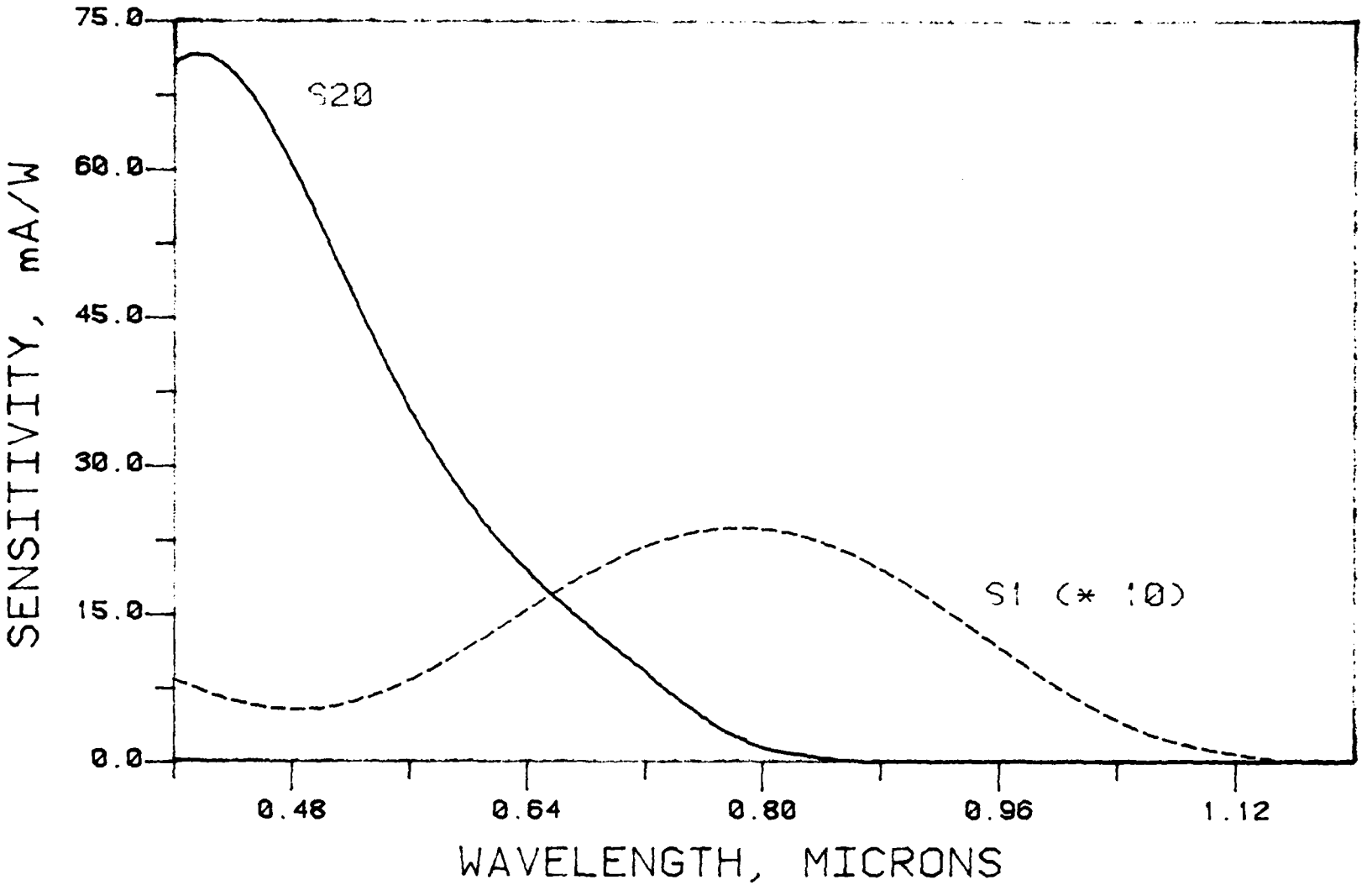

COMPARISON OF S20 AND S1 RESPONSES

Figure 11

range is desired, a proximity focused diode has been purchased with an S1 photo cathode and a P20 phosphor. By connecting the diode in front of the SIT, the OMA should have an S1 response and an intensified, gateable sensitivity up to wavelengths of about 1100 nm (see Figure 11). When the microscope optics and detector sensitivity are taken into account, a clear advantage appears for the S1 response when measuring the black body emission (see Figure 12). While the peak weld signals would be comparable for both photocathode responses, the S1 photocathode enables a wider wavelength range for the measurements (see Figure 13).

Vidicon detectors, while having a fairly linear response with continuous light intensity, have some characteristic non-linearities [3-4]. At high light levels, the detector becomes saturated and the response departs from linearity. Because of saturation and detector dark current, the effective light sensitivity range for the detector is about two orders of magnitude. Since the standard lamp is so much brighter than the black body and weld pool in the wavelength range of interest, means of reducing the lamp signal in a calibrated manner is needed.

Initially, various pin apertures were tried, but the results were not reproducible. It was later found that neutral density filters, if calibrated for transmission vs. wavelength, can be used to reduce the standard lamp light. The calibrated standard lamp values are then multiplied by the transmission values, and then divided by the lamp signals as before, to obtain the calibration constants for the system. If multiple neutral density filters are used, care must be taken to avoid internal reflections between filters.

The SIT detector response is linear with light intensity within $\pm$2%

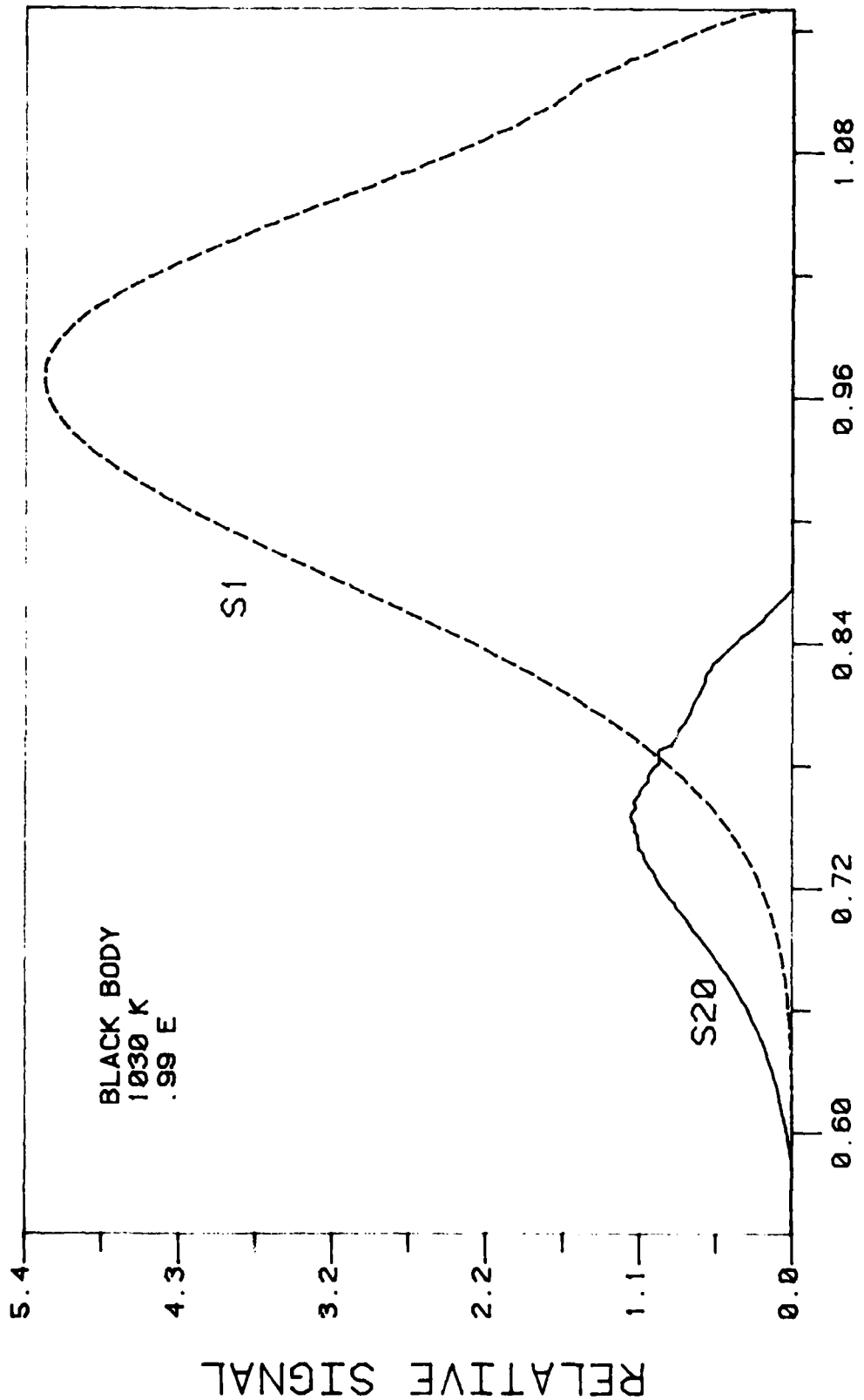
COMPARISON OF BLACK BODY SIGNALS
RELATIVE SIGNAL
5.4
4.3
3.2
2.2
1.1
0.0
WAVELENGTH, MICRONS
0.60
0.72
0.84
0.96
1.08
S1
S20
BLACK BODY
1030 K
.99 E

Figure 12

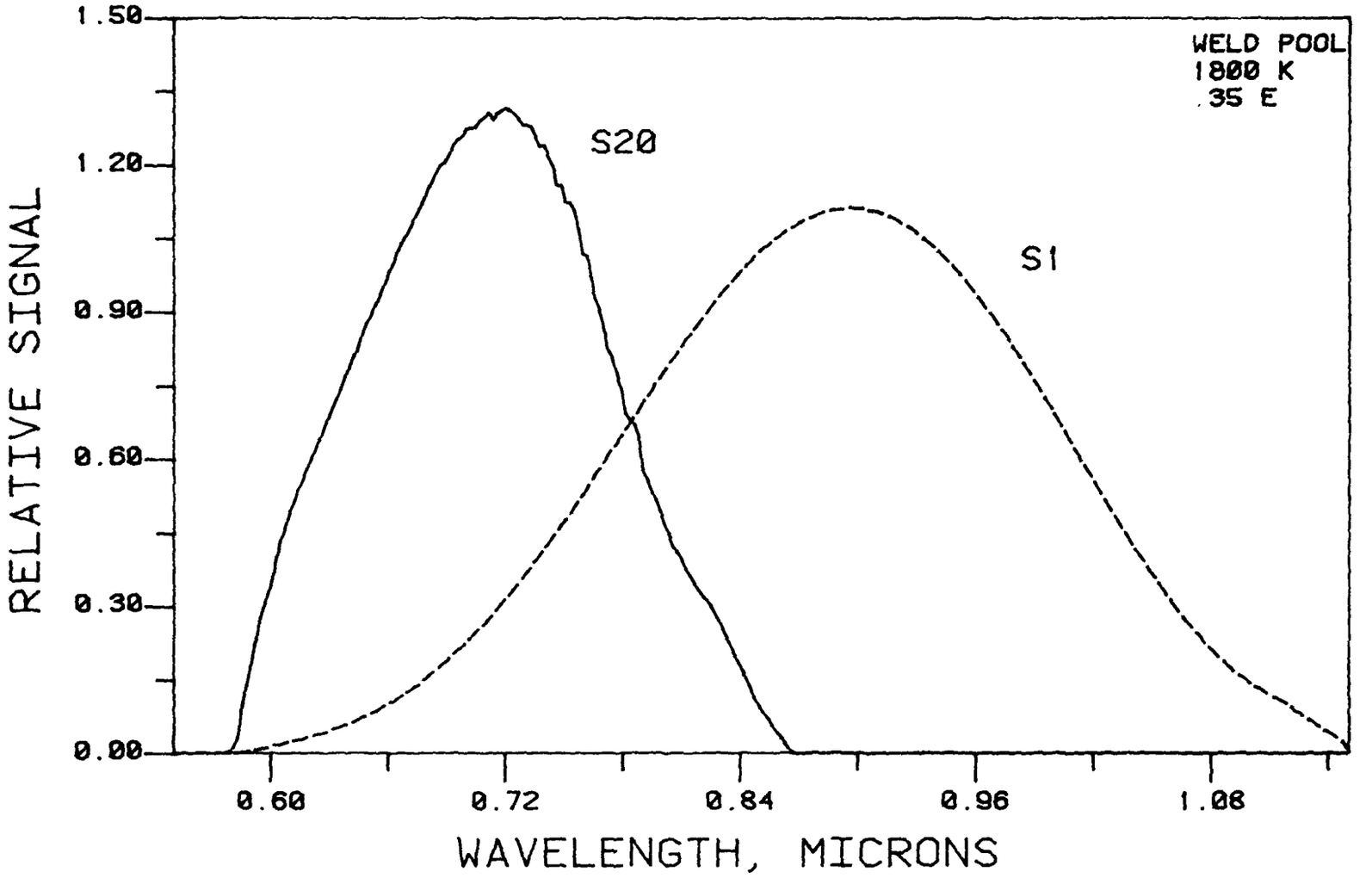

COMPARISON OF WELD POOL SIGNALS

Figure 13

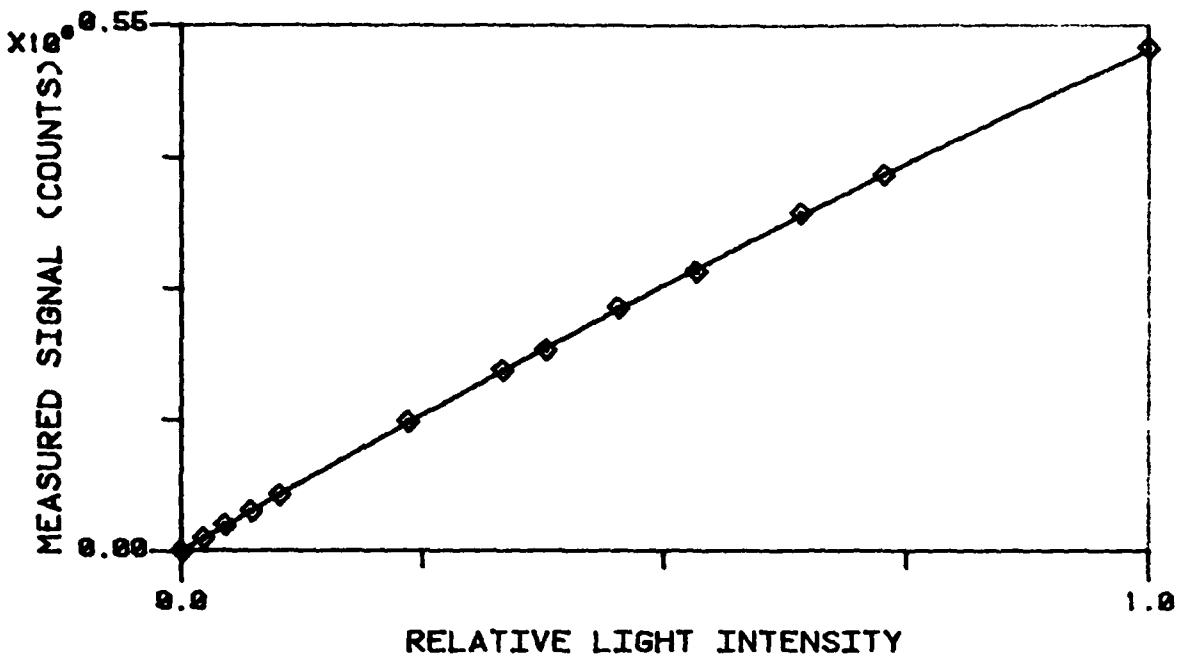

Figure 14 - SIGNAL TRANSFORMATION CURVE

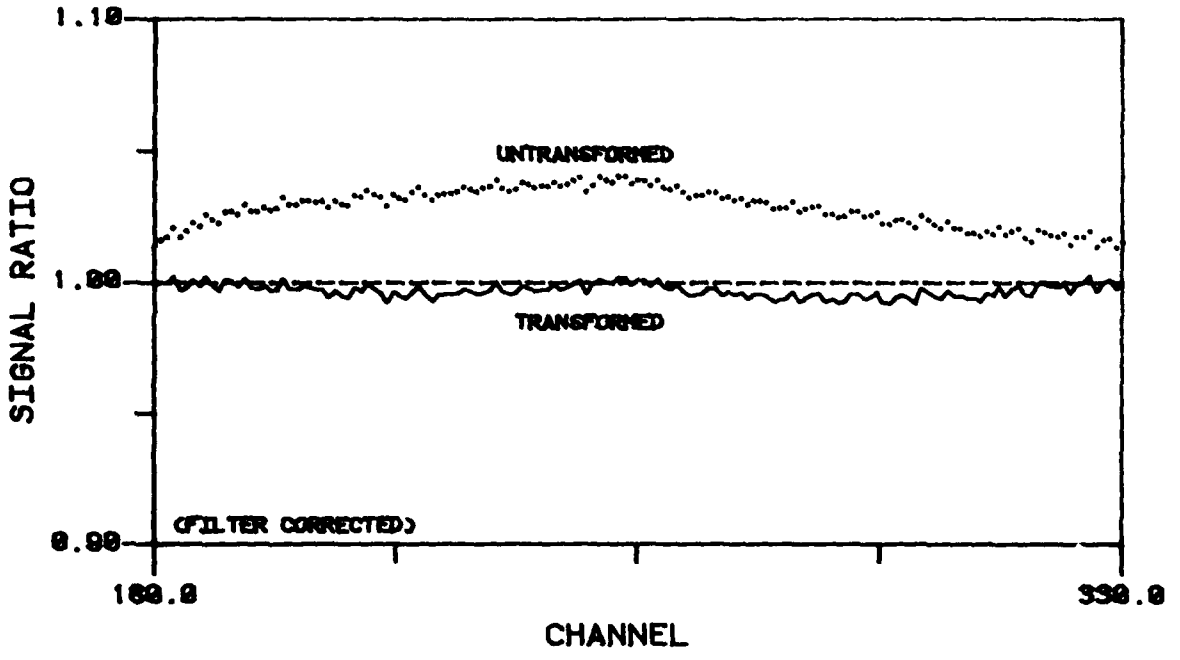

Figure 15 - SIGNAL RATIO CURVES

according to specification. However, the MIRTMA system is sensitive enough to be affected by the non-linear behavior which is systematic and is magnified by pulsed light sources [4]. The non-linearities associated with low light levels and pulsed sources can be corrected by adding a switching circuit to alter the detector voltage bias [5]. At medium light levels, however, transformation function is required to correct the measured signal to a linear scale prior to converting to spectral radiance values.

The calculation of the transformation curve for medium light intensities is baased on OMA measurements of the standard lamp using calibrated neutral density filters in the microscope. The OMA signal for each combination of filters at wavelength is recorded. The peak signal is arbitrarily assigned a transmission value of 1.00 (100% on a relative light intensity scale). Since the transmission at the particular wavelength is known for each measurement, all other signals can also be assigned transmission values relative to the peak signal transmission. A polynomial curve is then fited to these signal-transission data pairs to create the transformation curve. A typical transformation curve is shown in Figure 14.

Preliminary results have shown that the transformation function produced by this procedure is general to all channels of the SIT. The function is verified by ratios of transformed OMA signals taken using different combinations of calibrated filters. After correcting for the filters, the ratios should be nearly unity if the function is correct. Figure 5 shows a successful transformation of a series of measurements differing from a base series by a nominal filter density of 0.1

Work in the next year will complete the spectral radiance calibration proceedures, convert the SIT to an SI response, demonstrate the MIRTMA

system on a black body and begin temperature measurements of weld pools. It is believed that nearly all calibration procedures and systematic errors of this system have been completed and identified during the past year. As this facility becomes available, it should be useful in measuring the local surface temperature not only of weld pools, but of many other high temperature, high speed processes.

III. AUTOMATION OF WELDING

Automation is one area of welding technology that promises to pay tremendous dividends if high sensitivity, rugged sensors can be developed. One possible sensor is the arc itself, which is known to respond to geometric and chemical discontinuities at frequencies up to 20 kHz. In one study we are using digital signal analysis to measure these responses. In a second effort, the effects of surface depression and convection on weld pool shape and defect formation are being studied. These latter topics are of great importance in developing processes capable of producing weld pools of desired size and quality.

A. Signal Analysis of Welding Noise Voltage

Mr. C. D. Sorenson

The objective of this research is to use modern digital signal analysis techniques to determine natural oscillations occurring in the welding arc voltage and to attempt correlation of these signals with defects in the welds. Work was initiated in the spring of 1981 by purchase of a dedicated minicomuter. During the previous reporting period, the computer was brought on-line and a number of test welds were made which proved that disturbances to the welding process could be detected in either the time domain or in the frequency domain. Unfortunately, the noise level from the commercial welding power supply were of the same order of magnitude as the measured disturbannces. In the past year, a more sophisticated welding power supply has been designed and built, computer software and hardware have been upgraded, and signals from additional welds have been analyzed. The results continue to be encouraging, but the optimum signal analysis technique has

not yet been detemined.

The two greatest problems identified in the previous report period were the extraneous noise generated by the commercial welding power supply and this distortion caused by recording the welding voltage on magnetic tape. Both of these problems have been overcome in the current report period.

The first problem was overcome by acquiring a 600 amp DC (rms) transistorized current regulator manufactured by Alexander Kusko, Inc. This was delivered in January 1982; and after a period of initial testing, the regulator has proven extremely useful. The regulator can maintain a welding current constant to within 1%, thus permitting a high signal-to-noise ratio. The regulator is linear to more than 20 kHz which permits the use of precisely pulsed current when necessary. Figure 16 compares the current stability of a commercial constant current welding power supply with the regulator obtained with the Kusko supply. These tests were made on a large carbon block resistor. The coarse steps of ± 5 amperes are due to the sensitivity of the A/D converter used to record the signal. The actual regulation of the Kusko supply is better than ± 0.5 ampere at this current level.

The second problem of distortion of the signal by the AM magnetic tape has been corrected by software modifications to the computer which allow a direct 10 kHz sampling rate. Figure 17 shows a square wave as measured by the new direct input technique compared to the same square wave as recorded on the magnetic tape. The direct input technique is clearly superior.

In addition to these software improvements for direct input of the welding process data, a complete signal analysis package was acquired from Signal Technology, Inc. during the summer. This package has saved

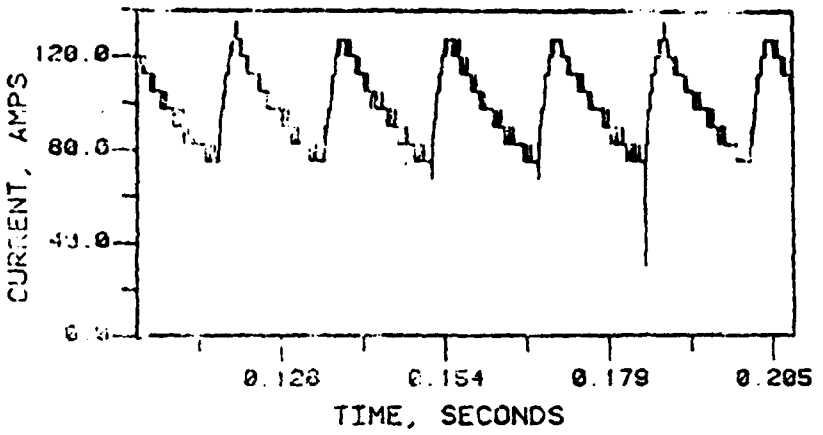

STANDARD DC POWER SUPPLY

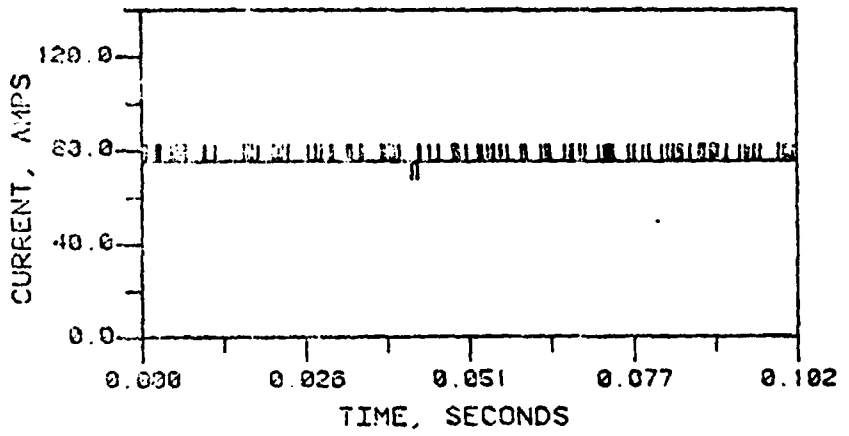

TRANSISTORIZED REGULATOR
WITH BATTERY

Figure 16

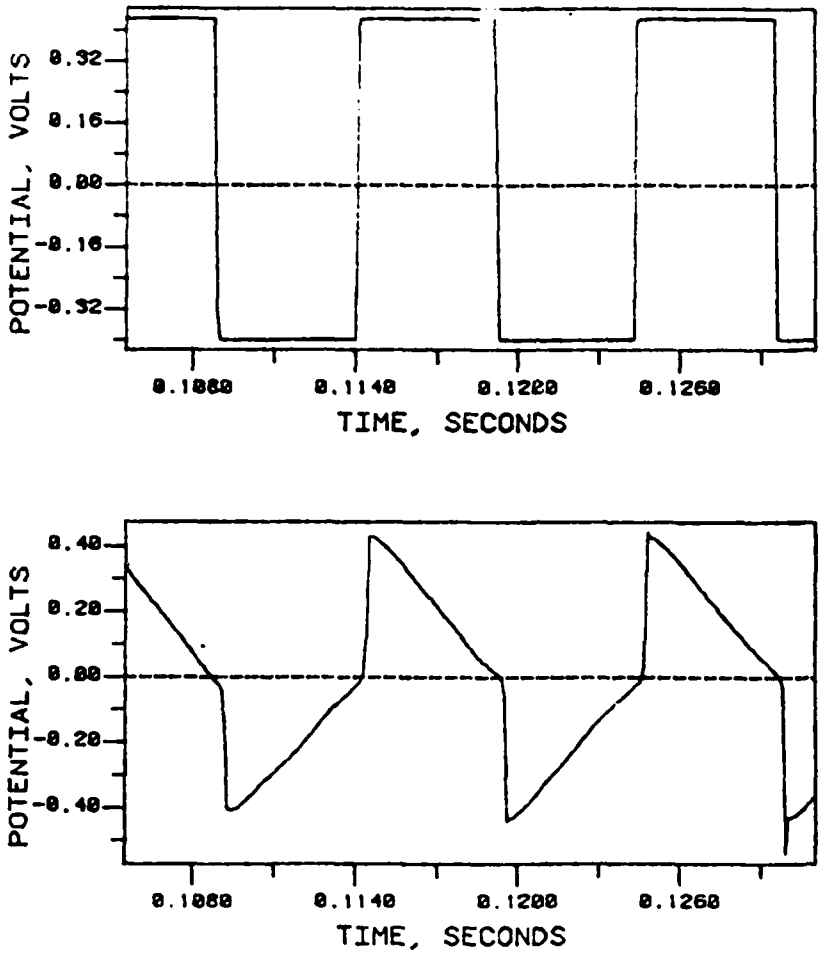

DIRECT INPUT (TOP)VS RECORDED INPUT (BOTTOM)

Figure 17

considerable time during the past few months by permitting emphasis on study of welds rather than on software development.

The initial welds were produced with constant welding current. Although this technique did produce measurable signals during the previous report period, recent tests have shown that this technique is not as sensitive as an impulse or square wave current signal. Figure 18 shows the frequency response of the welding voltage on a stainless steel plate and an aluminum plate at constant current. Although there are minor differences in the signal, the spectrum is generally only white noise. Figure 19 shows the spectrum on the same materials using a square wave current generated by the Kusko transistorized power supply. the harmonics of the square wave input are clearly observed, but it will be noted that the envelope surrounding the peaks of these harmonics is different for steel and for aluminum. A simple square wave response generates harmonic peaks which decay exponentially. This exponential decay is distorted for both aluminum and steel but in a different pattern for each. These patterns are very reproducible.

It was also noted that the DC arc voltage level varies between steel and aluminum. This is shown in Figure 20 which represents the shift in arc voltage when welding over a steel-aluminum laminate. These tests show, at least in principle, that welding over regions with chemical variations results in changes in the arc voltage. Studies have begun to test changes in voltage caused by welding over slag inclusions, but the results are inconclusive at present.

Figure 21 shows the change in arc voltage caused by minor disturbances in the shielding gas. These distributions are more readily observed in the time domain (Figure 21) than in the frequency domain (Figure 22).

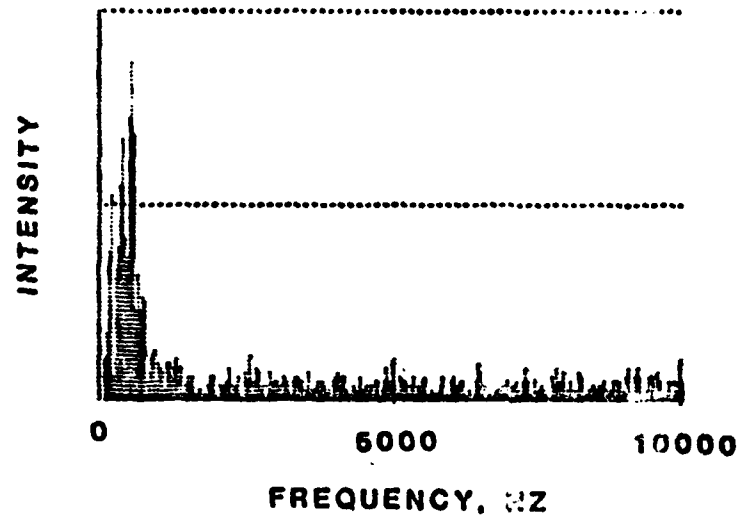

Steel

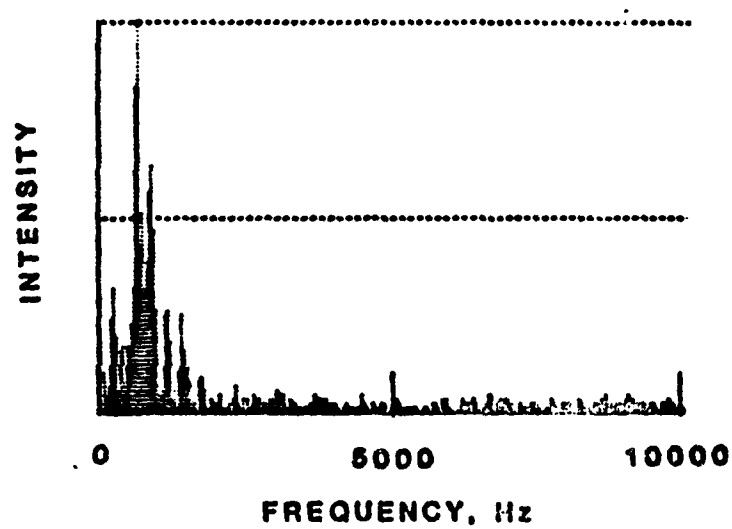

Aluminum

Magnitude transform of DC welds

Figure 18

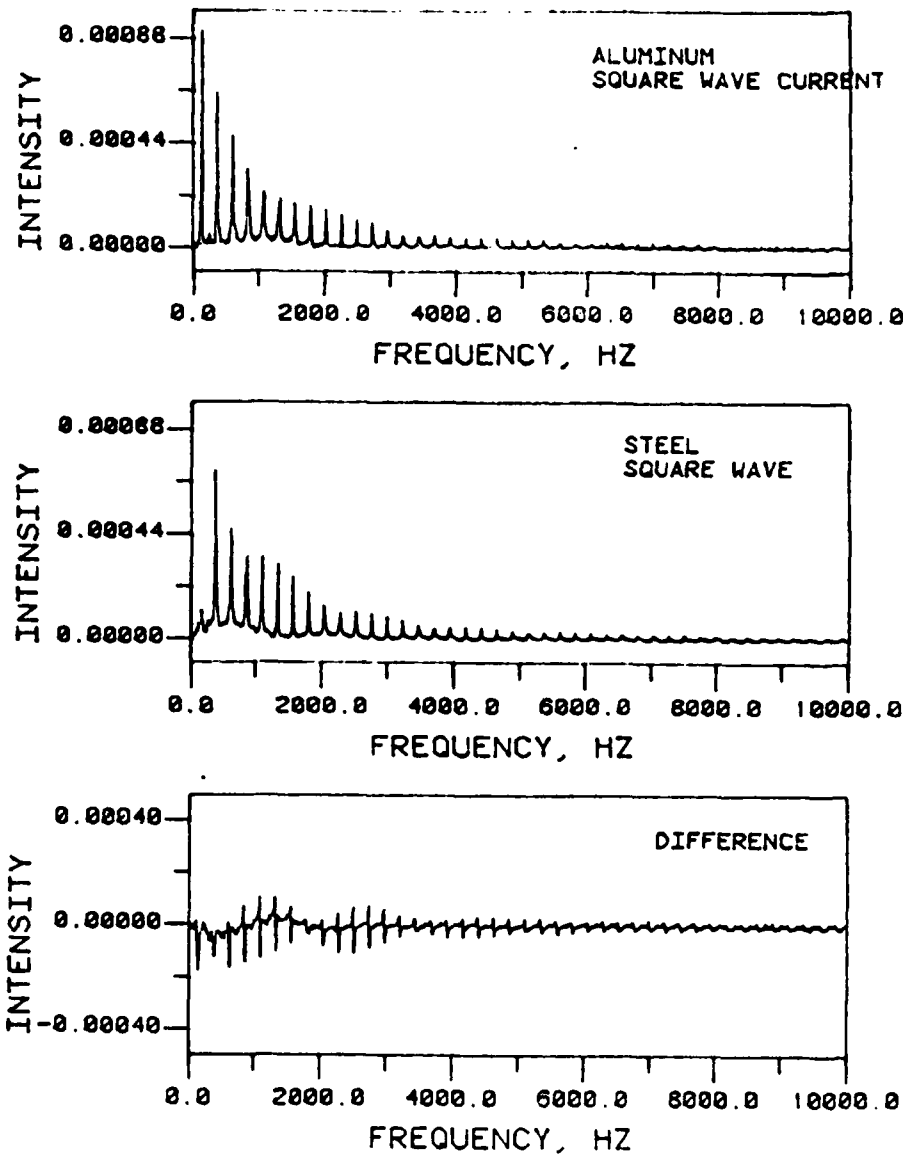

Magnitude Transform of Square Wave Welds

Figure 19

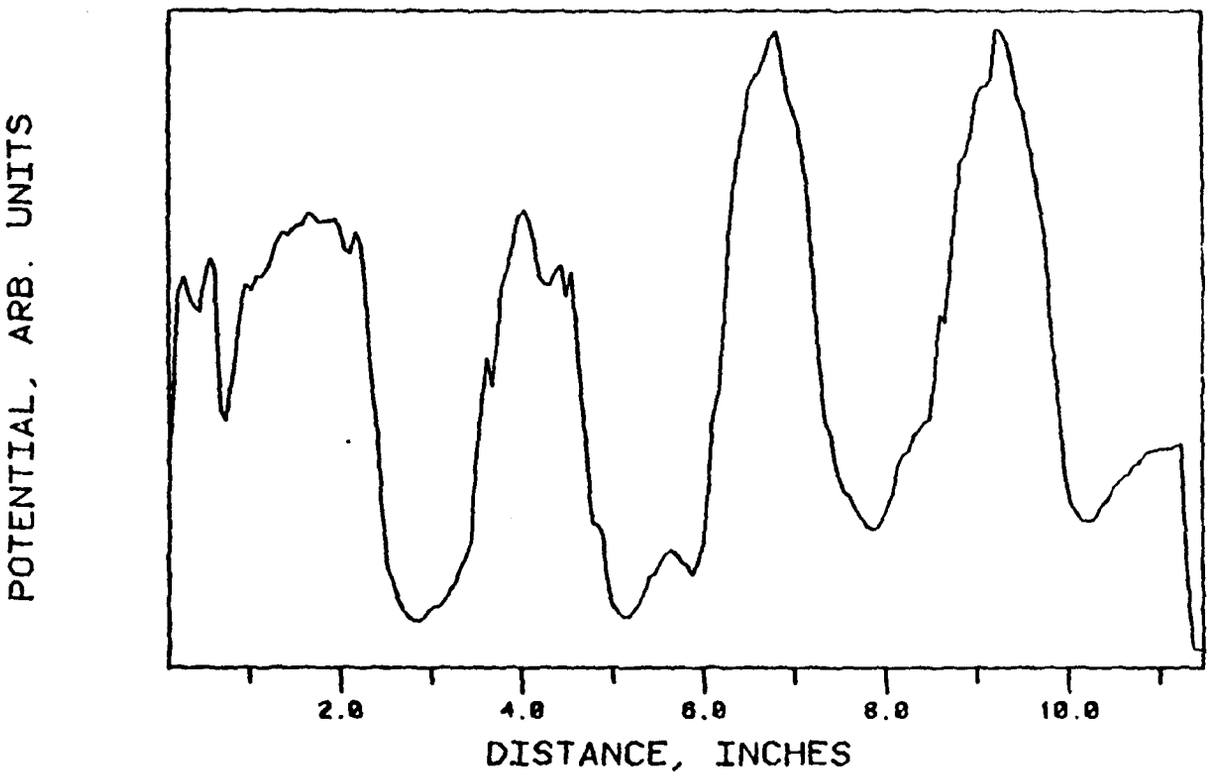

VOLTAGE CHANGES ACROSS A STEEL-ALUMINUM LAMINATE

Figure 20

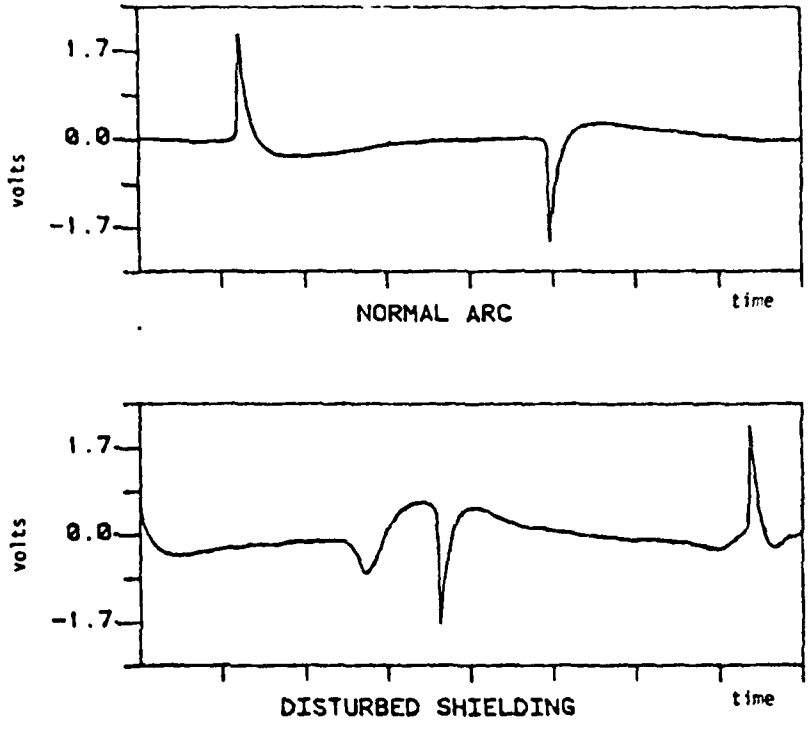

Figure 21: Effect of shielding gas on real time signal.

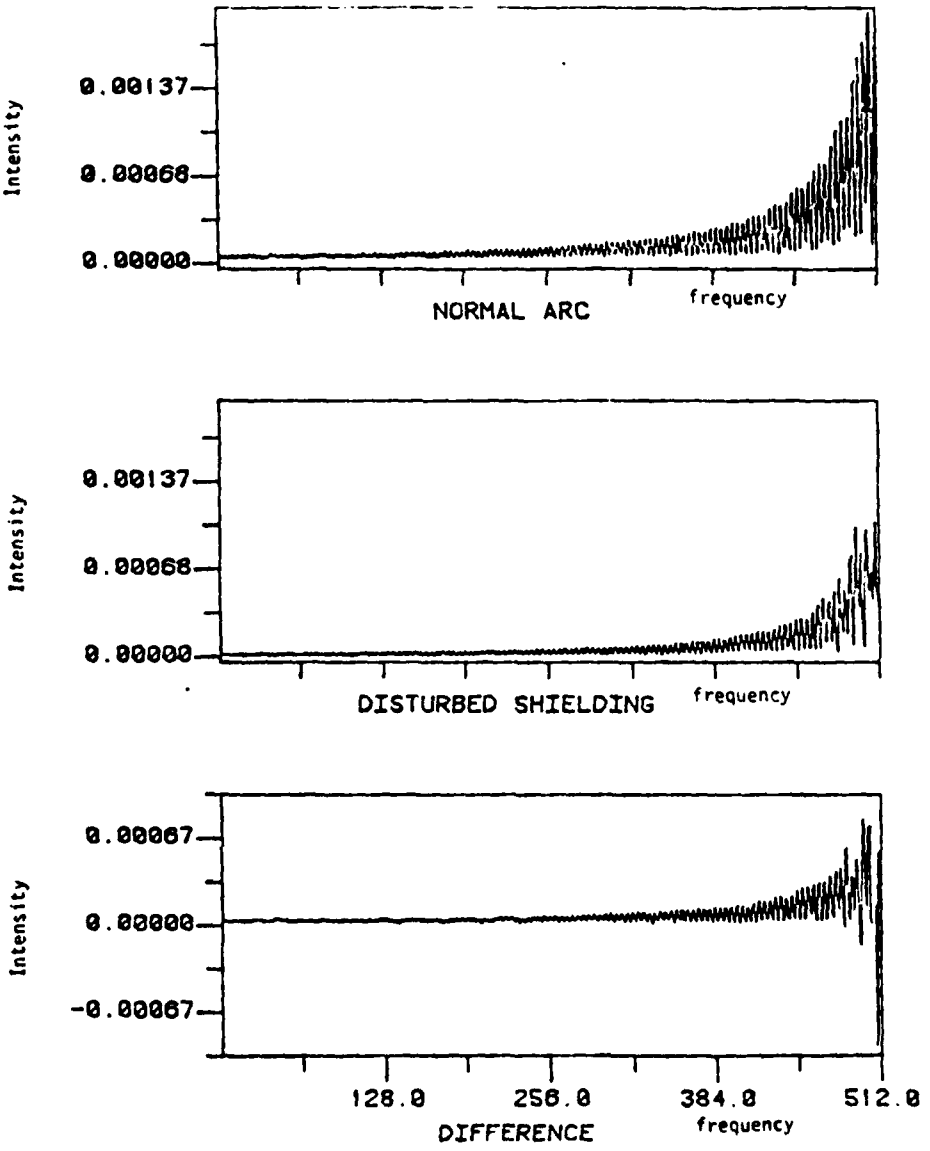

Figure 22: Effect of shielding gas on magnitude transform.

Progress has been made in both the welding equipment and in the signal analysis technique during the past year. The problems have been solved sufficiently that the project can concentrate on analysis of actual weldments during the current year. This will permit analysis of the frequency response of specific defects, as well as determination of the ultimate sensitivity of this control technique. In addition, welding signals will be analyzed by Nyquist plots in order to determine the transfer function for the process. These results will permit an accurate evaluation of the ultimate usefulness of this technique of weld quality monitoring.

B. Convection and Surface Depression of Arc Weld Pool

Mr. M. Lin

The purpose of this study is to determine the importance of weld pool depression and convection on weld pool geometry and defect formation in arc welding. Experiments were performed on 13 mm thick type 304 stainless steel plates. Stationary welds were measured after a dwell time of 3 seconds while moving welds were made over a wide range of velocities.

The effect of the current on the depth of surface depression is shown in the Figure 23. It is obvious that as the current increases the depth of surface depression increases significantly. It is found qualitatively that the surface depression depth is consistent with the observed metallographic penetration depth, and that the transition from shallow to deep surface depression occurs over a range of 20 amperes or less. For these deeply penetrated welds, the depth of surface depression can be a good indicator of the weld pool depth.

It is believed that the depth of surface depression cannot be totally

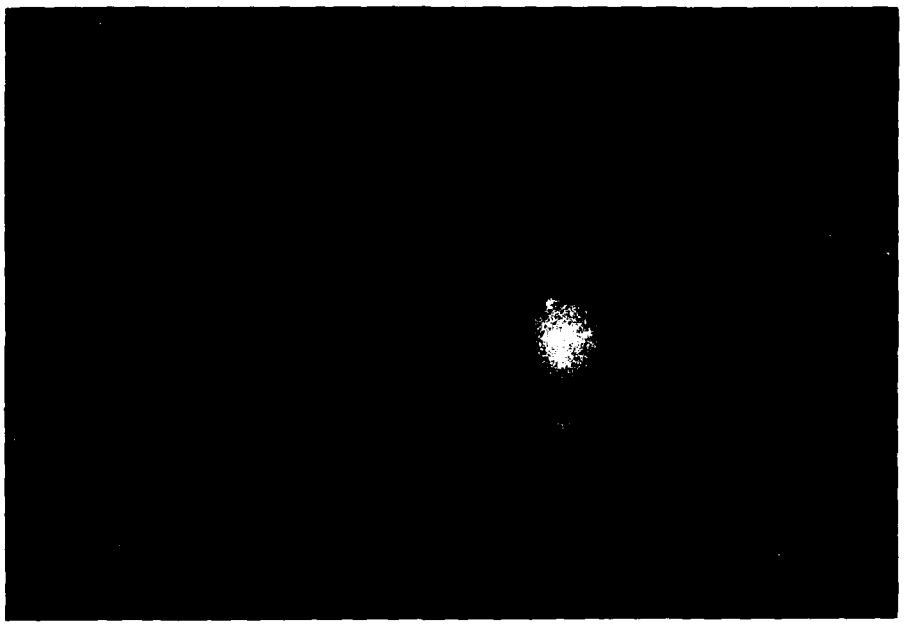

(a)

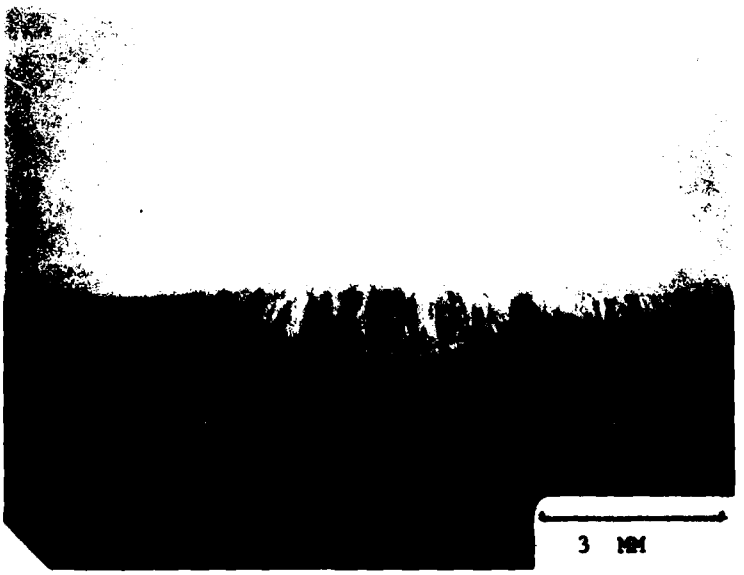

(b)

Figure 23: Comparison of the depth of surface depression to the penetration depth.
(a), (b) 235 amperes

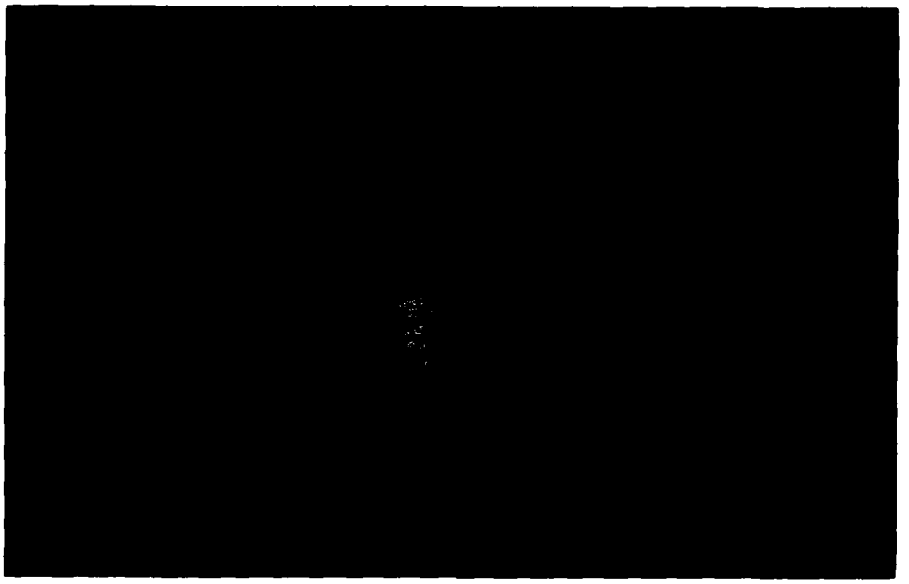

(c)

(d)

(c), (d): 285 amperes

(e)

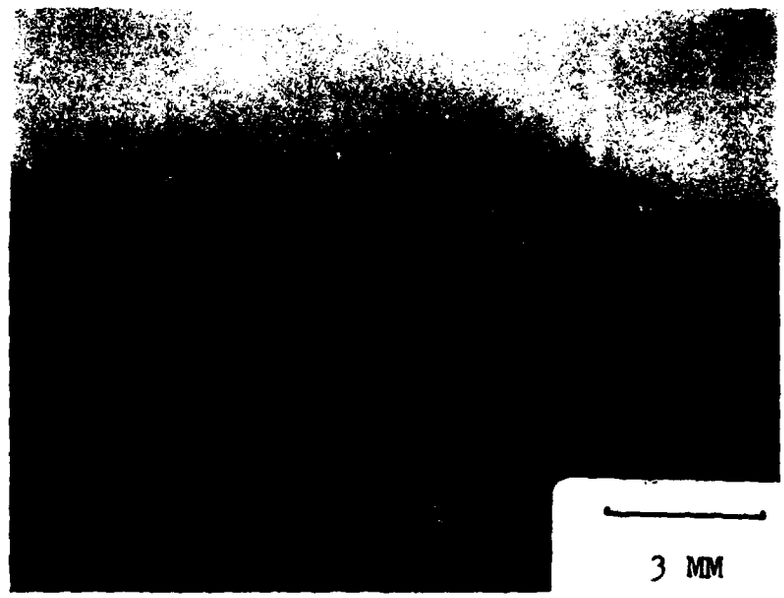

(f)

(e), (f): 335 amperes

explained by the balance of plasma jet gravitational and surface tension forces. Other factors such as vaporization of the base metal or vortex formation in the weld pool may explain the sharp increase of surface depression as current increases by only 20 amperes.

In stationary arc welding, once the deep depression is formed, the penetration depth does not increase even though the dwell time of the arc increases from 3 seconds to 40 seconds. The explanation may be that once the surface crater is formed, the current will be deflected to the sidewalls of the crater as shown in Figure 24. Since 80% of the heat is carried by the electrons, most of the heat will flow to the sidewalls of the crater. Thus, as dwell time increases, only the width of the weld pool is increased, and the depth of the weld pool is nearly constant.

A typical high current weld defect is a humped bead as shown in Figure 25. When the travel speed is less than 2 mm/sec, no humping is found and the weld pool shape does not differ from that observed in stationary arc welds. When travel speed increases, humping begins.

Figure 26 shows the development of an eddy flow behind the arc. In Figure 26, only a single eddy is seen, however, in high speed movies, double eddies behind the arc have been observed. The formation of eddies behind the arc may be due to electromagnetic forces which result from the nonuniformly distributed current in the weld pool. As shown in Figure 27, the current will tend to diverge when entering the liquid metal. The divergence will create a pressure gradient which drives the liquid metal downward at an angle. Because the electrical resistivity is greater in the liquid metal than in the solid metal, and the travelling arc weld pool is not symmetric, the current density is greater on the sides and in front of

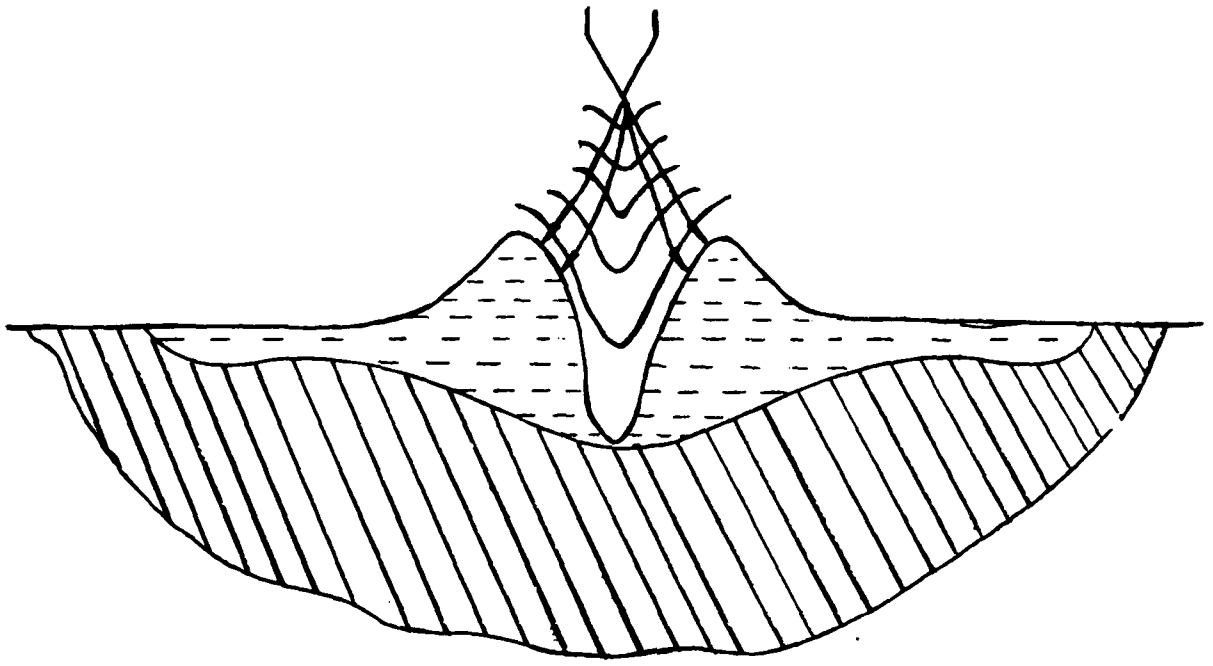

Figure 24: Schematic representation of the equipotential lines and the current flow paths.

Figure 25: Humping Beads

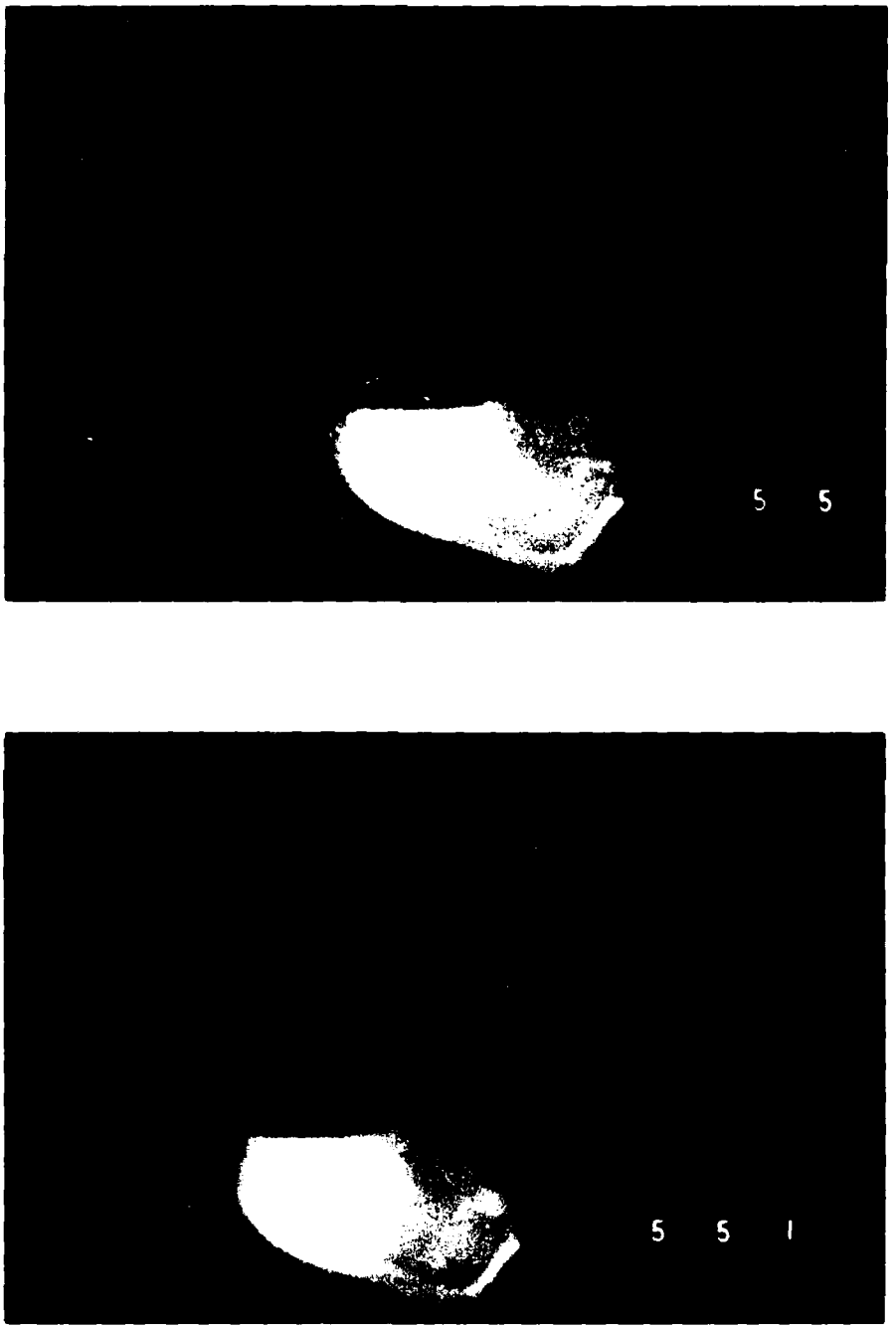

Figure 26: The sequence of formation of eddy behind the arc

the arc than behind the arc as sketched in Figure 27b. This maldistribution of current will form two eddies behind the arc. A single eddy may predominate when the current in the weld pool takes a preferential path to one side due to the electrical ground, asymmetric part geometry or some other reasons.

The forces most likey to produce defects are the surface tension force and the electromagnetic force. Surface tension forces push the liquid metal backward because the temperature in the front of the arc is higher than behind the arc, however, the eddies driven by the electromagnetic force push the liquid metal forward. Thus, in the initial state of formation of humping, surface tension forcs and electromagnetic forces compete to drive the liquid metal in opposite directions. In later stages, the liquid metal behind the arc becomes swollen, bringing it closer to the electrode and attracting more of the current to the liquid metal behind the arc. Finally, when most of the current flows to the humped weld bead behind the arc instead of flowing to the sides and the front parts of the arc, both the electromagnetic forces and the surface tension forces push the liquid metal backward and the metal is completely removed from underneath the arc. This bistable motion of fluid convection causes formation of humped beads.

Currently, the possible explanation of deep surface depresion due to vortex formation is being studied through a mathematical model.

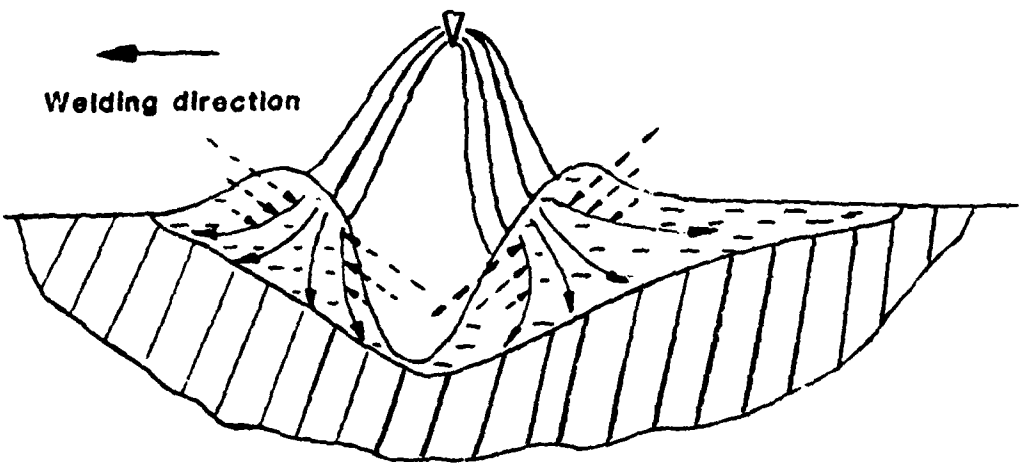

(a)

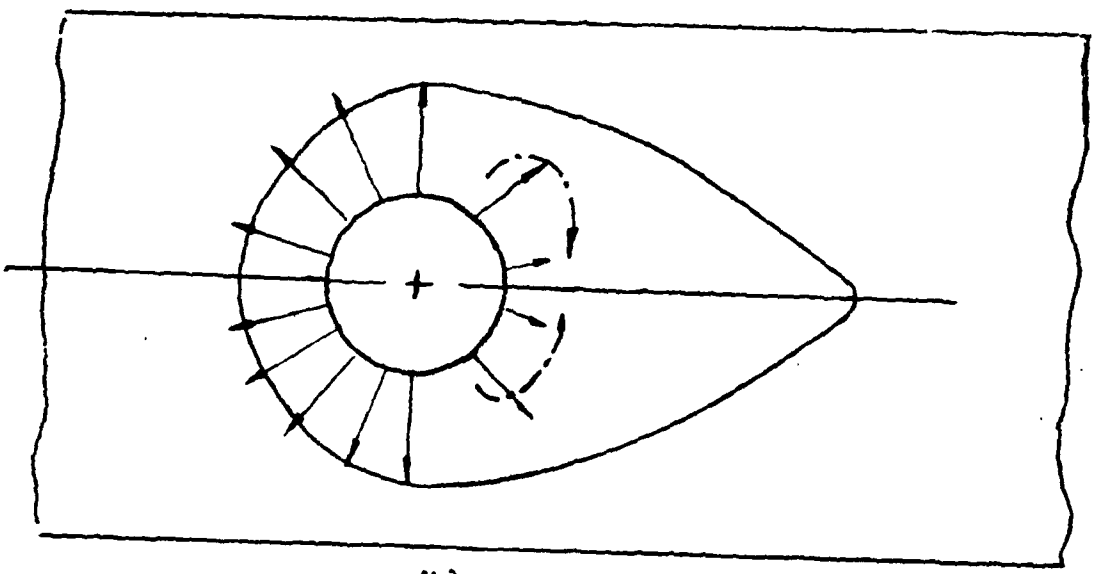

(b)

Figure 27: Schematic representation of the formation of humping caused by maldistribution current in the liquid pool which produces unbalanced electromagnetic forces.

IV. WELDING OF HEAVY SECTION TITANIUM

Joining of heavy section titanium is of particular concern to the Navy for advanced systems. In the previous year's report, initial studies of electroslag welding and pulsed current gas-metal arc welding were described. During the past year, the work on electroslag welding has been completed with new contracts being let to MSNW, Inc., Oregon Graduate Center and Prof. D. Sadoway at MIT. We have consulted with each of these new contractors to ensure a smooth transfer of knowledge gained in this program to these continuing efforts.

During the past year, the pulsed current gas metal arc welding equipment has become operational, and welding has begun.

A. Electroslag Welding of Titanium

Mr. S. K. Fan

Electroslag welding of titanium is potentially very attractive due to the high deposition rates which can be obtained. During the previous reporting period, it was found through computer modeling and limited experimental work that pure CaF_2 fluxes did not provide a heat distribution in the slag pool capable of fully diluting the base metal under normal operating conditions. Based upon a survey of other potential fluxes, a series of fourteen titanium electroslag welds were made during the past year using CaF_2-SrF_2 based fluxes. Dilution was still poor as shown in Table 1 which lists values from none to 16 percent. The SrF_2 fluxes produced better results than pure CaF_2 but further work is necessary to develop even better flux systems for ESW of titanium.

Weld No.	1	2	3	4	5
geometry (cm)					
width	2.1	2.3	1.8	1.8	1.8
thickness	2.2	2.2	2.2	2.2	2.2
height	8.9	10.2	14.0	19.1	14.0
voltage (Volts)	20	20	20	20	17
current (Amperes)	400	400	400	400	450
flux (wt %)					
CaF_2	70	85	80	50	50
SrF_2	30	15	20	50	50
completion time (sec)	197	225	230	200	260
electrode (3 mm. diam.) feedrate (cm/sec)	2.7	2.9	3.0	4.7	2.7
dilution, percent	7	2	11	9	12

Table 1: Welding conditions and dilution for fourteen titanium electroslag welds.

Weld No.	6	7	8	9	10
geometry (cm)					
width	1.8	1.8	1.8	1.9	1.8
thickness	2.2	2.2	2.2	4.4	2.2
height	14.0	14.5	15.2	17.8	24.0
voltage (Volts)	20	20	20	15	20
current (Amperes)	600	500	500	600	200 | 500
flux (wt %)					
CaF_2	20	0	0	50	50
SrF_2	80	100	100	50	50
completion time (sec)	170	145	175	357	840
electrode feedrate (cm/sec)	4.1	5.0	4.3	5.3	1.4
dilution, percent	5	2	5	9	-

Table 1: (continued)

Weld No.	11	12	13	14
geometry (cm)				
width	1.5	1.5	1.5	1.5
thickness	2.2	2.2	2.2	2.2
height	17.1	15.2	17.8	17.8
voltage (Volts)	20	17	20	17
current (Amperes)	400	500	450	400
flux (wt %)				
CaF_2	0	50	100 (commercial purity	0
SrF_2	100	50	0	100
completion time (sec)	260	270	245	250
electrode feedrate (cm/sec)	2.7	2.3	3.0	2.9
dilution, percent	16	10	-	14

Table 1: (continued)

During the past year, a new ONR project on such flux development has begun with Prof. D. Sadoway at MIT. Another project on ESW of Ti has been given to Oregon Graduate Center. After conferring with each of these new contractors and with ONR, it was agreed that no further ESW Ti work will be performed under this contract at this time.

B. Pulsed Current Gas-Metal Arc Welding of Titanium

Lt. D. Ries, USN

Gas Metal Arc Welding of titanium is being investigated using the analong current regulator built by Alexander Kusko, as described in a previous report [1]. This current regulator has the capability of producing pulsed current waveforms up to 20 kHz of practically any shape available from a signal generator. The objective of this work is to achieve control of metal transfer so that the molten filler metal is incorporated into the weld pool in a controlled, orderly fashion with a minimum of spatter. Normally, with DC current conventional GMA produces uncontrolled and unbalanced arc forces which tend to hamper controlled metal transfer when welding titanium. These unbalanced forces result in weld pool turbulance, uncontrolled droplet transfer and ultimately nonuniform weld bead formation. The use of rectangular pulsed current waveforms is being investigated with respect to metal transfer control and ultimate weld bead shape and uniformity.

The experimental space consists of three independent variables including base current (I_b), peak current (I_p) and frequency, keeping the average current constant. Average current (I_{av}) is chosen based on the minimum DC level which produces a desired weld bead size. By changing the

energy input at constant I_{av} using rectangular pulsed wave forms, changes in metal droplet transfer and resulting weld bead profile are recorded. The experimental technique used for recording metal droplet transfer consists of high speed photography (6,000 frames per second) using a balance of laser back lighting and arc illumination to record the formation and time-of-flight of individual droplets. An attempt is being made to record the current signal on the film next to each high speed picture to allow real time analysis of droplet transfer as a function of pulsed current input. To date, this technique has been successfully used to record metal droplet transfer with aluminum at 260A DC, 50 Hz 200-300A square wave pulse and 500 Hz 200-300A square wave pulse. Data will be analyzed using a multi-frequency level Box-Behnken design space grid allowing for statistical analysis of dependent variables including weld bead cross section dimensions and area, weld pool size, wire feed rate, relative percent spatter and soot, and relative weld bead uniformity.

A heat transfer model is being developed to predict weld bead geometry. The heat transfer model applies a superposition of a gaussian distributed heat source from Tsai's work at MIT on gas tungsten arc welding with a step heat input representing heat transferred to the weld pool by I^2R heating plus electron heating at the wire tip. This provides a modified distributed heat source which may be used to define an operating parameter and ultimately an estimation of weld bead size. These estimations will be evaluated with respect to experimental results which are underway.

All welding is being performed in an argon purged glove box with a titanium getter furnace cleansing system for removal of O_2, H_2, H_2O, and N_2. Interesting results using this system for welding 1100 aluminum have been

recorded with respect to the effect of argon flow rate, O_2 level in the shield gas and O_2 level around the shield gas on weld porosity and cathodic cleaning ahead of the arc. These results are summaried as follows:

1. Ar flow rates from 0 to 1.0 cfm were used with 50 Hz 200-300A square wave pulse current wave form. At no external flow rate weld metal transfer is unstable and gross weld porosity is present with no cathodic cleaning. As flow rates are increased cathodic cleaning increases and porosity decreases.
2. Adding O_2 to the Ar shielding gas at low flow rates which otherwise result in poor weld control, appears to stabilize metal transfer and increase cathodic cleaning.
3. Adding O_2 ahead of the Ar shield appears to increase the efficiency of cathodic cleaning around the weld bead.

These effects may be the result of either or both of the following phenomena:

1. Increased sputtering yield from Ar shield gas due to small amounts of O_2.
2. Surface reaction of O_2 with hydrated oxide species and/or hydrocarbon contaminants removing oxides and contaminants from the surface.

Further studies of this effect of oxygen on cathodic cleaning of aluminum are being held pending further results of GMAW of titanium. During the past year the entire glove box, GMAW transistorized welding power

supply, laser back-lighted high speed photography system has become operational and welds have been made on Al and Ti. Thus far only the effect of oxygen on cathodic cleaning of aluminum has resulted from these tests, but much more information on the fundamentals of metal transfer in pulsed GMAW is expected in the next year now that this facility is fully operational.

V. FRACTURE TOUGHNESS OF HY-80 WELDMENTS

Two projects were initiated during the previous year's contract period in collaboration with General Dynamics Electric Boat Division. In these studies GDEB provides data, material, machine work and charpy testing while MIT produces the weldments and analyzes the results. One project involves an evaluation of the toughness of HY-80 weld metals produced at high heat inputs with Oerlikon OP121TT and Lincoln 880 fluxes. The second project is investigating the effect of nitrogen in the weld metal on strain aging as a possible cause of loss of toughness on the first side of a double V groove weld.

A. Fluxes for High Heat Input Submerged Arc Welding

Lt. Cdr. B. Wilson, USN and Mr. A. Oladipupo

We have studied the effect of welding variables, namely, current, voltage and travel speed on the fracture toughness of HY-80 weld metal using two commercial fluxes, Lincoln 880 and OP121TT. We also tested these fluxes to determine the reasons for their reported differences in fracture toughness.

The experimental work was directed towards correlating the variables of voltage, current and travel speed to fracture toughness. An equation predicting charpy values based on regression analysis using the scaled values of voltage (V), current (I), and travel speed (T) was obtained (see Table 2 for coefficients for each flux).

The conclusions of these tests were as follows:

1. Voltage, current and travel speed variations play a significant role in the toughness of the weld metal.

Table 2

EQUATIONS PREDICTING CHARPY VALUE BASED ON REGRESSION ANALYSIS USING THE SCALED VALUES OF VOLTAGE(V), CURRENT(I) AND TRAVEL SPEED(T)

$$CV\ (ft\ lbs) = X0 + X1(V) + X2(I) + X3(T) + X4(V \times I) + X5(V \times T) + X6(I \times T) + X7(V^2) + X8(I^2) + X9(T^2)$$

WHERE 30 TO 36 VOLTS IS SCALED TO -1 TO 1
400 TO 500 AMPERES IS SCALED TO -1 TO 1
12 TO 18 IN/MIN IS SCALED TO -1 TO 1

COEFFICIENT	LINCOLN 880	OP121TT
X0	71.1111	69.7778
X1	-3.8333	-3.6250
X2	13.5417	5.2083
X3	8.2083	11.6667
X4	1.7500	-3.8333
X5	-8.5833	-6.2500
X6	-2.0000	0.5833
X7	-10.0556	-.3056
X8	-2.9722	-9.4722
X9	-4.9722	-1.3889
R-SQUARED	56.3%	68.8%
PURE ERROR	34.7%	24.6%
LACK OF FIT	9.0%	6.6%
STANDARD DEV OF PREDICTION (FT LBS)	13.88	8.72

2. The loss of Mn in the welding arc can be reduced or eliminated if the flux contains MnO. (See Figure 28 and Table 3).
3. The heat input does not uniquely control the weld metal toughness but heat input below 2 KJ/min is more detrimental than is heat input above this level. (See Table 4).

We have also studied weld-metal transformation behavior of some welds made from Lincoln 880 and OP121TT. Gas-Tungsten Arc remelt welding was used to study the order of appearance of the different microphases.

A Pt/Pt-13%Rh thermocouple shielded in twin-bore alumina refractory tube and with reference at 0°C was placed in the weld pool immediately behind the arc. After some time, the weld and frozen-in thermocouple were quenched in water held at room temperature. Cooling curves were obtained from the thermocouple connected to an X-t chart recorder. These curves were used to estimate temperatures at various distances behind the arc. Longitudinal sections along the GTA weld were polished and etched in 4% picral and 5 ml HCL for 15 seconds. Light microscopy was used to study the microphases, (see Figure 29). Acicular ferrite, proeutectoid ferrite, widmanstaten side plates and retained austenite can be observed in this figure; however, no correlation of fracture toughness with optical microstructure has been found. Differential thermal analysis (DTA) was performed on welds made with Lincoln 880 in hope of correlating transformation temperatures and fracture toughness. Cylindrical specimens 2.4 mm in diameter and 4.5 mm in length were machined from each weldment.

Specimens were cleaned in acetone and alcohol to remove grease and dirt. They were finally cleaned ultrasonically in a detergent solution. A nominal 10°C/min heating rate and 100°C/min cooling rate were used. The

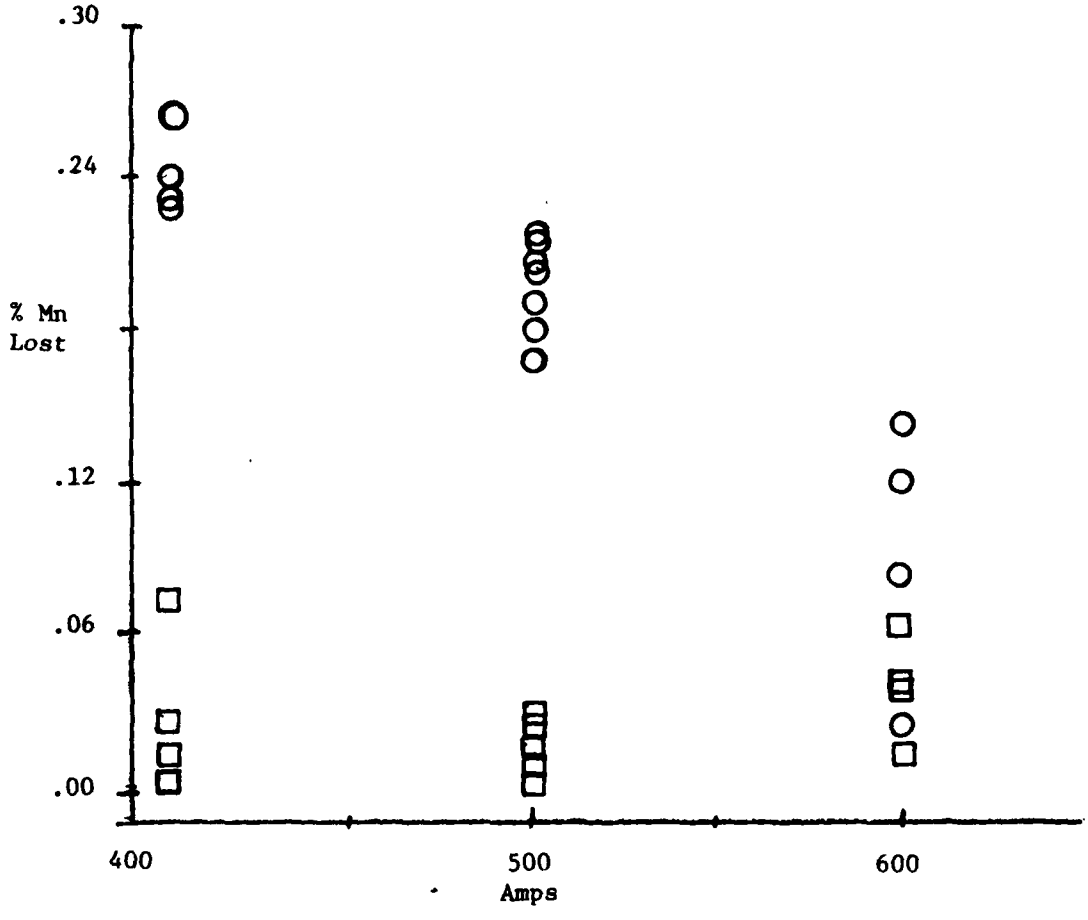

Figure 28: Manganese lost to the slag as a function of welding current.

○ Lincoln 880

□ OP 121 TT

Table 3

REPORTED FLUX COMPOSITIONS

COMPOUND	LINCOLN 300 WT PERCENT		OP121TT WT PERCENT			
ANALYSIS	(A)	(B)	(C)	(D)	(E)	(F)
REFERENCE	[31]	[33]	[32]	[30]	[34]	[35]
SiO_2	16.0	13.9	15.6	13.5	13.4	15.0
MnO	NONE	NONE	1.9	1.8	0.9	? *
CaO	3.0	2.1	7.0	8.0	11.0	? *
MgO	27.0	26.3	25.7	43.6	40.0	? *
Al_2O_3	22.0	22.7	19.2	18.1	14.2	? *
TiO_2	2.0	NONE	1.1	1.0	0.5	? *
CaF_2	22.0	22.7	26.5	20.99	14.4	25.0
ZrO_2	4.0	7.4	NONE	0.2	NONE	NONE
FeO	NONE	1.0	NONE	NONE	1.7	NONE
Na_2O	NONE	2.0	NONE	NONE	0.9	NONE
K_2O	NONE	NONE	NONE	0.2	0.8	NONE
BaO	NONE	NONE	NONE	NONE	0.1	NONE

$$* SiO_2 + TiO_2 = 15.0$$

$$CaO + MgO = 35.0$$

$$Al_2O_3 + MnO = 20.0$$

The above analyses are from the literature and have in most cases been based on the assumption that all the elements are in an oxide form. This assumption therefore will not show the presence of the binding agent which is probably a potassium or sodium silicate. The actual form of the compounds is most likely much different, for example it is known that Lincoln 880 contains ZrO_2 as a zirconium silicate.

Table 4

THE EFFECT OF HEAT INPUT VARIATIONS

ON THE TOUGHNESS

	VOLTS	AMPS	TRVSPD in/min	HEAT INPUT KJ/mm	PREDICTED CV LINCOLN 880		OP121TT	
					Joules	(ft lbs)		
MINIMUM HEAT INPUT	30	400	18	1.58	87	(64)	96	(71)
OPTIMUM HEAT INPUT	31	575	18	2.4	114	(84)	119	(87)
MAXIMUM HEAT INPUT	36	600	12	4.25	91	(67)	68	(50)

The loss in Cv divided by the difference in heat input for the extremes shown above are

	LINCOLN 880	OP121TT
INCREASE IN HEAT	14.6 J/KJ/mm	12.4 J/KJ/mm
DECREASE IN HEAT	28.1	62.2

Clearly the decrease in heat input from the optimum is much worse for toughness than is the same increase above the optimum.

furnace atmosphere was argon at a flow rate of 52 cc/min. Figure 30 shows the typical heating and cooling curves obtained. Temperatures read off the graph are characteristic temperature (T_x), peak temperature (during heating)(T_p), and the temperature at which the air blast turned on during the heat cycle (T_s). Peak areas were evaluated and overlapping curves were separated using L. G. Berg's [8] technique, (see Table 5).

The characteristic temperatures were obtained using Murray and Fischer's techniques [6]. Forty-five degree tangents were drawn to the knees of the curves and points of tangency give the characteristic temperatures. During the cooling cycle there were two transformations conforming with microphases identified in Figure 29, namely proeutectoid ferrite and acicular ferrite. This is in agreement with P.E.L.B. Rodriques, and J. H. Robinson [7].

Even through the charpy values ranged from 43 to 83 (ft lbs), there was no significant difference in transformation temperatures as seen in Table 5.

During the past year, the relative fracture toughness of HY-80 submerged arc welds made with Lincoln 880 and Olerikon OP121TT have been measured with surprisingly little difference in the results. The OP121TT samples had less scatter in the results, but the Lincoln 880 was capable of producing welds of equivalent toughness to the best obtained with the Olerlikon flux. Further studies of structure and transformation temperatures have failed to distinguish the factors controlling toughness in these weld metals. Further quantitative metallography will be performed on the welds. The quantitative metallography will be used to determine the amounts of all microphases observed in hopes of elucidating the primary features controlling the toughness.

Table 5

Test	Volt (V)	Amps (A)	CV (ft lbs)	T_{xh} (C°)	T_p (C°)	T_s (C°)	T_{xC1} (C°)	T_{xC2} (C°)	TVSP (in/min)
2	33	500	45	710	735	810	695	565	15
3	30	500	50	710	735	810	695	567.5	12
4	30	500	83	720	747.5	808	710	530	18
7	33	600	76	715	737.5	810	690	567.5	12
8	33	600	78	710	727.5	810	690	567.5	18
9	36	500	43	705	730.0	810	690	580	12
11	33	500	79	712.5	735.0	805	690	572.5	15
13	30	400	48	710	735	810	695	560	15
14	30	600	62	710	732.5	809	680	580	15
15	33	500	80	712	730	810	690	570	15
16	36	400	54	725	747.8	810	717.5	537.4	15

T_{xh} = characteristic temperature on heating curve

T_{xC1}= characteristic temperature on first peak during cooling cycle

T_{xC2}= characteristic temperature on second peak during cooling cycle

Figure 29: Weld 5 showing proeutectoid ferrite (PF). acicular ferrite (AF), and retained austenite (RA), (x500).

B. The Effect of Nitrogen on Weld Metal Toughness

[Although some work was performed on this topic during the past year the student working on this has been expelled from MIT for disciplinary reasons unrelated to his research. As a result of this unfortunate incident and the unfriendly departure of the student, no results are available to be reported. Continuation of this project is postponed until new personnel are found].

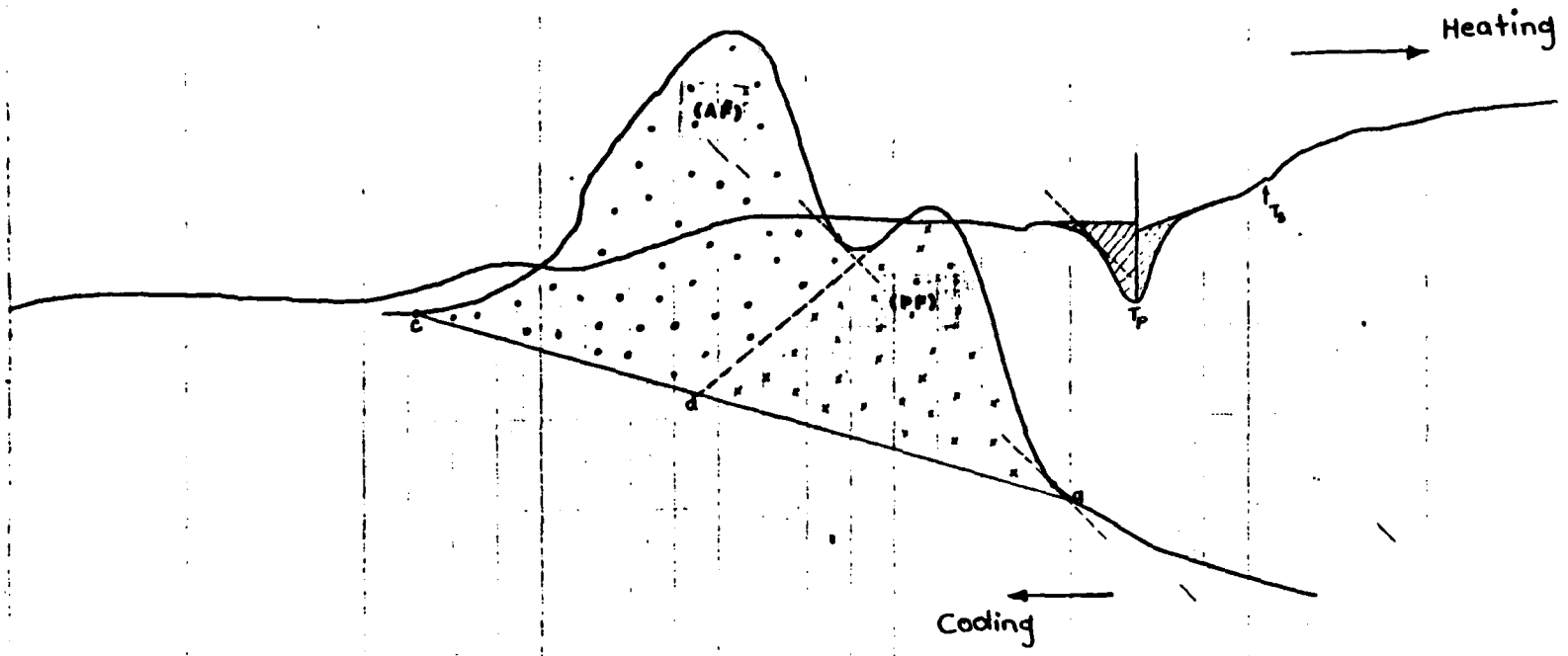

	✓ 5		100	100	T-7-ω
			1000	970	
				10	02-08-83
	99.95% Cu metal	Ar	52	max	Bisi

Figure 30: In cooling cycle, first peak is due to proeutectoid ferrite (PF) and second to acicular ferrite (AF).

SUMMARY

During the past year, significant progress has been made in our studies of spectroscopy of arc welding, automation, fluid flow and weld pools and welding of heavy section titanium. The results of studies of fracture toughness of HY-80 have been less fruitfull and the effort in this area will be reduced over the coming year so that efforts can be concentrated in the more promising research topics.

REFERENCES

1. T. W. Eagar et al., "Heat Source--Materials Interactions During Fusion Welding," Second Annual Technical Report, Contract N00014-80-C-0384, April 30, 1982.

2. A. Block-Bolten and T. W. Eagar, "Selective Evaporation of Metals From Weld Pools," Trends in Welding Research in the United States, ASM, Metals Park, OH, pp. 53-62.

3. Y. Arata, S. Miyake, H. Matsuoka and H. Kishmoto, "Two-dimensional Multichannel Spectroscopy of a Pulsed Arc," Trans. JWRL, 10, (1), 1081, pp. 33-38.

4. G. W. Liesegang and P. D. Smith, "Vidicon Characteristics Under Continuous and Pulsed Illumination," App. Op., 21, (8), April 1982, pp. 1437-1444.

5. H. E. Cascio, P. D. Smith, and G. W. Liesegang, "Simple Switching Circuit to Improve Vidicon (OMA 2) Linearity," Rev. Sci. Instrum., 53(7), July 1982, pg. 967-968.

6. J. A. Murray and H. C. Fischer, Proc. Am. Soc. Test. Mater., 51, pp. 1197-1212.

7. P.E.L.B. Rodriques and J. H. Rogerson, "How Weld Metal Thermal Cycles Determine the Toughnes of Submerged Arc Welds," Welding and Metal Fabrication, April 1980, pp. 183-190.

8. L. G. Berg, "On Area Measurements in Thermograms for Quantitative Estimations and Determination of Heats of Reaction", Comptes Rendus (Doklady) de l'Academie des Sciences de l'URSS, Vol. XVIX, No. 9, 1945, pp. 648-651.

9. Mackenzie, Differential Thermal Analysis, Vol. 1, Academic Press, London, 19790, pp. 45-59.

10. D. J. Widgery, "Deoxidation Practice for Mild Steel Weld Metal," Welding Research Supplement, pp. 57s.